Nagoya, Japan), and analyses of the photographs were performed with an automatic cell analysis system attached to the microscope. Data concerning patient age, sex, presence of guttae, and ECD were recorded. The eyes were classified into four groups by slit lamp examination according to modified Stocker's classification[9]:

Stage 1: Guttata cornea without the stroma or the epithelium being affected

Stage 2: Permeation of corneal stroma with fluid, edema of epithelium, and bullae formation

Stage 3: Late stages with subepithelial connective tissue formation, vascularization, and scar formation

Other eyes without corneal guttae were classified as stage 0. During the rest of the article, the term Fuchs' corneal dystrophy (FCD) represents stage 2 and 3, since eyes in these stages have symptoms related to corneal edema. The study complied with the Declaration of Helsinki. Approval was granted by the Committee for the Protection of Human Subjects of each hospital.

Mathematical Model of Endothelial Cell Loss Rate

To construct a mathematical model of decrease in endothelial cells, we made the following two assumptions:

1. The ECD at 5 years of age is 3600 cells/mm^2. This is common to all classes.
2. From 5 years of age, the decrease rate (percent/year) of ECD is constant in each class, but different between classes.

Murphy et al.[10] reported that during first 2 years of life ECD decreased rapidly because of corneal growth, and after that the decrease rate slows down to 0.56%/year. The effect of corneal growth on ECD ends at 5 years of age or earlier. To simplify our mathematical model, we assumed that ECD at 5 years of age was common to all classes and regarded this point as the base point of age-ECD curve in our mathematical model. Because the onset of FCD is in adulthood, we believe that this assumption is acceptable. We substituted the mean ECD of normal 5-year-old children (3600 cells/mm^2) in the report of Nucci et al.[11] for the base point. We assumed that the (percentage) decrease rate is dependent on the class, and it is constant in each class from 5 years of age. Based on these assumptions, the following differential equation stands:

$$dE_{(t)}/d(t) = -(D/100) \cdot E_{(t)}$$

$$E_{(t=0)} = 3600$$

where t is age 5 years; $E_{(t)}$ is endothelial cell density at t years (in cells per square millimeter); and D is the decrease rate (percent).

The solution to the differential equation is the following:

$$E_{(t)} = 3600e^{[-(D/100)t]}$$

Using this mathematical model, an age-ECD curve in each class can be drawn by the least-squares method. An age–ECD curve of optimal decrease rate can be drawn as well.

Statistical Analysis

Scatterplotting, analysis of variance (ANOVA), nonparametric density smoothing, age-ECD curve, and other statistical analyses were calculated by or written in commercial software (Excel 2007; Microsoft, Redmond, WA, and JMP 8 software; SAS, Cary, NC). $P < 0.05$ was considered statistically significant.

Results

Characteristics of Patients

Age, sex, and stage of reviewed patients and eyes are presented in Table 1. The prevalence of guttata cornea (stage 1+2+3) was 12.73%. The prevalence of stage 1 was 10.65%, and FCD (stage 2+3) was 2.08%. The male: female ratio in each stage was as follows; 1: 1.03 (stage 0), 1: 1.88 (stage 1), 1: 2.43 (stage 2), and 1: 4.67 (stage 3). Females were more predisposed to stage 1 or FCD than males, and the ratio increased in advanced stages.

Age-ECD Curve of 2.0% Differentiates Fuchs' Dystrophy

Figure 1, left shows the scatterplot between age and ECD for each stage. Nonparametric density smoothing was drawn on the scatterplot (Fig. 1, right), which represents the contour of plot density. The age-ECD curves based on our mathematical model were drawn by the least-squares method. Table 2 shows ECD with sample sizes at 5-year intervals for grades 0 to 3, which enables the mean ECD data of grade 0 to 3 to be compared at various ages.

The decreased rate curve of stage 1 age-ECD was 0.81%, which was closer to that of stage 0 (decrease rate, 0.44%) than that of stage 2 (2.65%) or stage 3 (3.08%). The decrease rate of stage 0 in our study was 0.44%, which is within the range of

Table 1. The Age, Sex, and Stages of Reviewed Patients and Eyes

Patient Stage	Age, y (Mean ± SD)	Male (*n*)	Female (*n*)	Total (*n*)	Prevalence (%) Total	Male	Female
0	65.3 ± 16.2	848	872	1720			
1	68.5 ± 14.3	73	137	210	10.65	7.84	13.17
2	70.3 ± 10.6	7	17	24	1.22] 2.08	0.75] 1.07	1.63] 2.98
3	75.1 ± 12.4	3	14	17	0.86]	0.32]	1.35]
Total	66.6 ± 15.4	931	1040	1971	12.73	8.91	16.15

Eye Stage	Male (*n*)	Female (*n*)	Total (*n*)
0	1426	1483	2909
1	103	205	308
2	13	28	41
3	5	18	23
Total	1547	1734	3281

Prevalence of FCD was calculated as sum of stage 2 and 3. In this table, if a patient had eyes in different stages, then he or she was classified in the severer of the stages between the eyes.

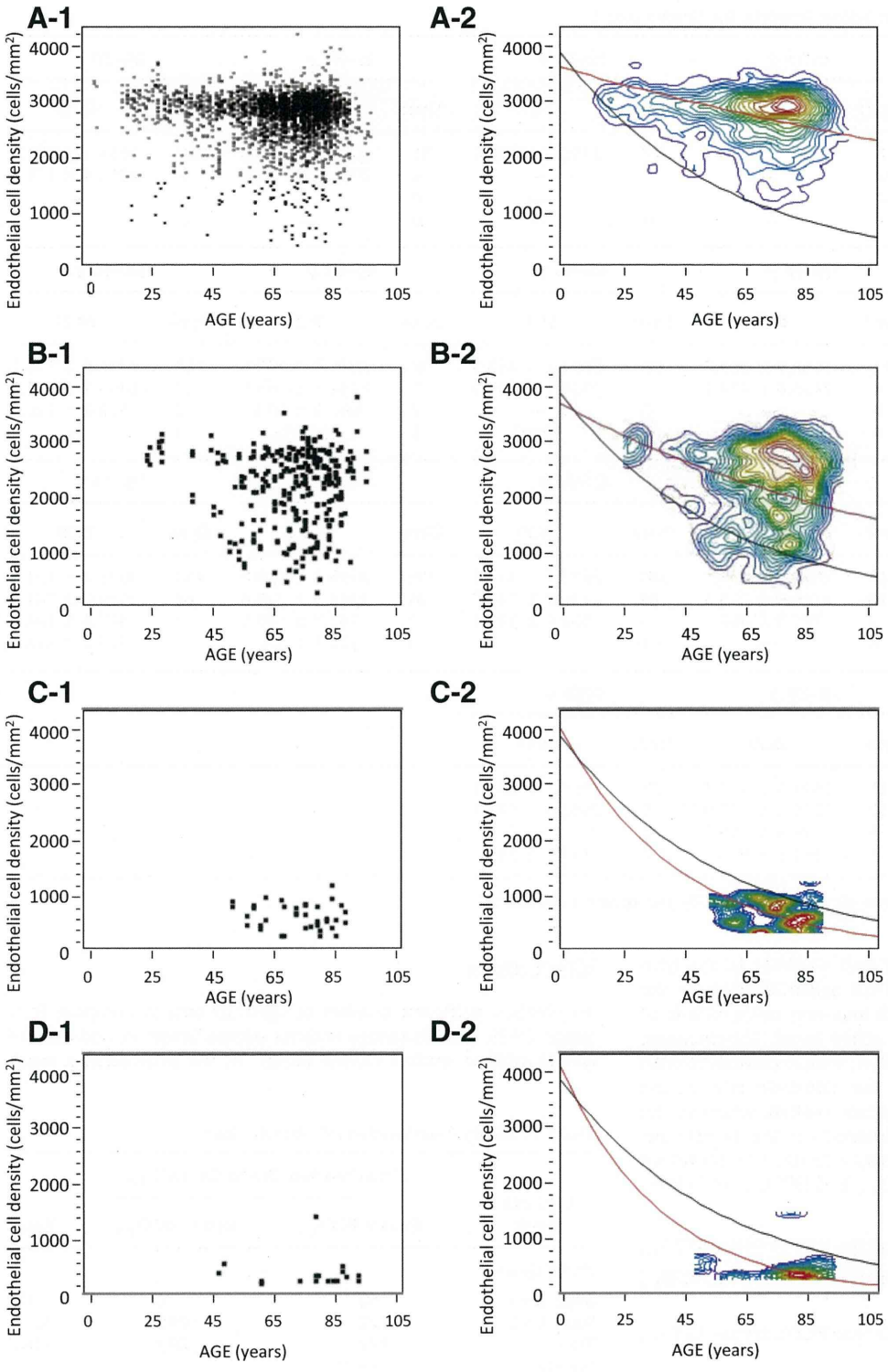

FIGURE 1. Scatterplots (*left*) and contour maps of nonparametric density smoothing (*right*) of each stage. (**A-1**, **A-2**) Stage 0, (**B-1**, **B-2**) stage 1, (**C-1**, **C-2**) stage 2, and (**D-1**, **D-2**) stage 3. *Red curves*: age-ECD curves of each stage calculated by least-squares method. The decrease rates of each stage were 0.44% (stage 0), 0.81% (stage 1), 2.65% (stage 2), and 3.08% (stage 3). The contour maps showed that the age-ECD curve of 2.00% decrease rate ($ECO_{2.0}$, *black curves*) ran through a trough between peaks of all stages. Most of the peaks in stages 0 and 1 were located above $ECO_{2.0}$, whereas peaks of stages 2 and 3 were located below $ECO_{2.0}$.

normal eyes reported in previous studies (Table 3).[10,12–16] Contour maps show that most of the peaks in stage 0 and 1 were located above the age-ECD curve of the 2.00% decrease rate, whereas peaks of stage 2 and 3 were located below this curve. Table 4 shows binary classification based on the age-ECD curve of a 2.00% decrease rate, designated novel ECD cutoff 2 ($ECO_{2.0}$), dividing stages 0+1 and stages 2+3 (Table 4) or stage 1 and stages 2+3 (Table 4). The high sensitivity and specificity of these classifications suggested that $ECO_{2.0}$ is an adequate cutoff between eyes with corneal edema and those without edema.

Age-ECD Curve of 1.4% and 2.0% Divides Stage 1 into Three Distinct Groups

The contour map of stage 1 consisted of several peaks. Figure 2 shows that the age-ECD curve of the 1.40% decrease rate, designated novel ECD-cutoff point 1 ($ECO_{1.4}$), divides these peaks into a high-density group ($>ECO_{1.4}$), and a low-density group ($<ECO_{1.4}$). ANOVA revealed that the age-ECD curves of each group predicted ECD according to age, with statistical significance: The *F* ratio and *P* value were 803.3 and <0.0001

TABLE 2. Mean ECD with Sample Sizes at 5-Year Intervals for Grades 0 to 3

	0–9 y		10–14 y		15–19 y		20–24 y		25–29 y	
	Eyes	ECD	Eyes	ECD	Eyes	ECD	Eyes	ECD	Eyes	ECD
Stage 0	4	3073.3 ± 392.6	7	3020.4 ± 330.1	47	2769.2 ± 530.1	31	2837.4 ± 567.3	60	2853.1 ± 507.6
Stage 1	0	—	0	—	0	—	4	2765.0 ± 128.8	6	2954.5 ± 175.6
Stage 2	0	—	0	—	0	—	0	—	0	—
Stage 3	0	—	0	—	0	—	0	—	0	—
	30–34 y		35–39 y		40–44 y		45–49 y		50–54 y	
	Eyes	ECD	Eyes	ECD	Eyes	ECD	Eyes	ECD	Eyes	ECD
Stage 0	58	2732.6 ± 511.3	54	2741.9 ± 324.7	80	2672.2 ± 462.5	99	2687.8 ± 507.8	128	2754.6 ± 370.5
Stage 1	0	—	4	2423.0 ± 474.1	7	2503.7 ± 541.9	7	1934.3 ± 763.9	14	1865.2 ± 703.0
Stage 2	0	—	0	—	0	—	2	881.0 ± 60.8	2	592.0 ± 120.2
Stage 3	0	—	0	—	1	461.0	1	622.0	0	—
	55–59 y		60–64 y		65–69 y		70–74 y		75–79 y	
	Eyes	ECD	Eyes	ECD	Eyes	ECD	Eyes	ECD	Eyes	ECD
Stage 0	195	2701.2 ± 408.1	325	2671.9 ± 464.4	384	2677.7 ± 449.1	494	2698.4 ± 435.0	496	2691.2 ± 421.3
Stage 1	25	2105.2 ± 673.3	28	2219.4 ± 695.5	39	2124.8 ± 743.7	61	2242.5 ± 719.4	44	2159.0 ± 741.7
Stage 2	4	645.8 ± 224.3	2	797.5 ± 282.1	7	562.9 ± 329.5	7	730.7 ± 149.5	7	483.0 ± 183.7
Stage 3	2	284.5 ± 21.9	0	—	0	—	2	302.5 ± 3.5	7	524.0 ± 418.9
	80–84 y		85–89 y		≥90 y					
	Eyes	ECD	Eyes	ECD	Eyes	ECD				
Stage 0	309	2698.9 ± 440.4	116	2624.5 ± 457.3	22	2563.7 ± 299.3				
Stage 1	47	2264.2 ± 556.2	17	2279.2 ± 597.9	5	2962.0 ± 597.1				
Stage 2	7	680.6 ± 318.1	3	723.3 ± 155.7	0	—				
Stage 3	5	302.4 ± 5.4	3	482.3 ± 97.1	2	352.5 ± 74.2				

Eye data are expressed as the number, and the ECD in cells per square millimeter.

in the high-density group and 945.7 and <0.0001 in the low-density group. The decrease rate of the age-ECD curve in the high-density group was 0.56%, which was very close to that of the stage 0 age-ECD curve. On the other hand, the decrease rate in the low-density group was 2.00%, which coincided with $ECO_{2.0}$. These results suggest that the decrease rate of the high-density group in stage 1 was nearly normal, whereas the low-density group in stage 1 was located on the border between eyes with and without corneal edema. We therefore classified stage 1 on the basis of $ECO_{1.4}$ and $ECO_{2.0}$, as follows (Fig. 3):

Stage 1a, asymptomatic guttata cornea (AGC): above $ECO_{1.4}$

Stage 1b, borderline guttata cornea (BGC): between $ECO_{1.4}$ and $ECO_{2.0}$

Stage 1c, preliminary stage of FCD (pre-FCD): below $ECO_{2.0}$

TABLE 3. Decrease Rates of Stage 0 in the Present Study and Normal Unoperated Eyes Reported in the Previous Studies

Author	Decrease Rate (%/y)	Nation
Murphy et al.[10]	0.56	United States
Cheng et al.[12]	1.00	England
Ambrose et al.[13]	0.60	England
Numa et al.[14]	0.30	Japan
Bourne et al.[15]	0.60	United States
Rao et al.[16]	0.30	India
Present study	0.44	Japan

DISCUSSION

To obtain a sufficient number of age-ECD data to compare FCD (stage 2+3), guttata cornea without edema (stage 1), and control group without guttata cornea (stage 0), we performed a retro-

TABLE 4. Binary Classification of Clinical Stage

Clinical Stage	Classification Based On $ECO_{2.0}$		
	Below $ECO_{2.0}$	Above $ECO_{2.0}$	Total
Total Eyes			
Stage 2+3	60	4	64
Stage 0+1	122	3095	3217
Total	182	3099	3281
Sensitivity, %	93.75		
Specificity, %	96.21		
Eyes with Guttata Cornea			
Stage 2+3	60	4	64
Stage 1	27	281	308
Total	87	285	372
Sensitivity, %	93.75		
Specificity, %	91.23		

Data are based on the age-ECD curve of 2.00% decrease rate as a novel ECD-cut-off ($ECO_{2.0}$), sensitivity and specificity to detect stage 2+3 from total eyes or the eyes with guttata cornea based on the classification.

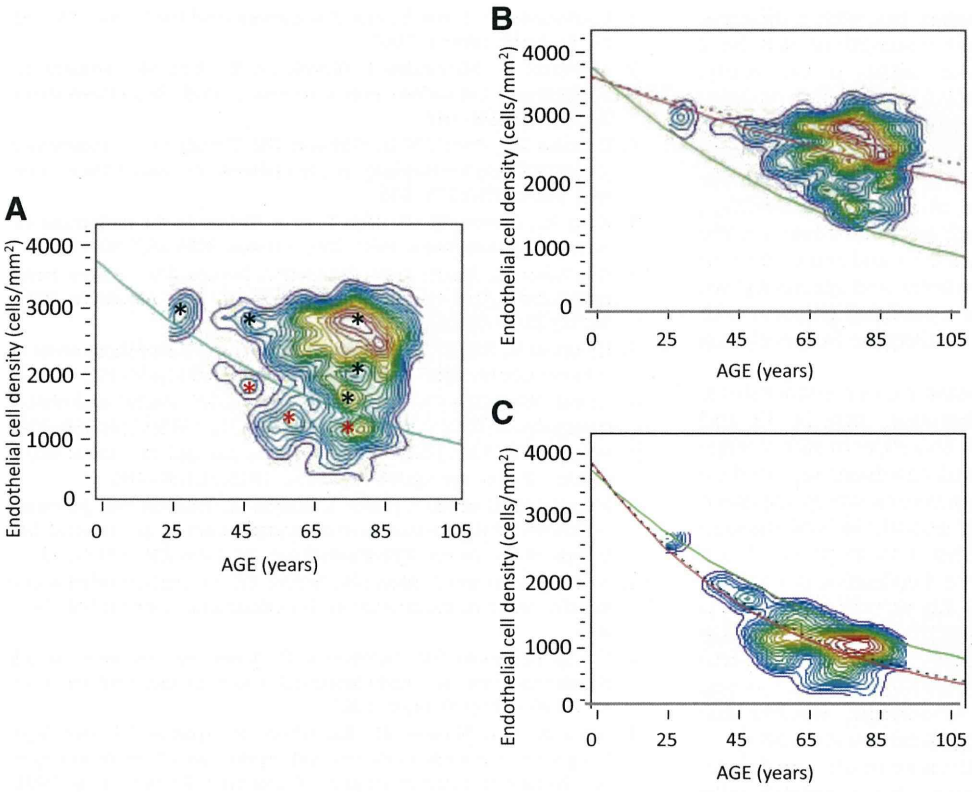

Figure 2. (**A**) The contour map of nonparametric density smoothing in stage 1. Stage 1 consisted of several peaks, and the age-ECD curve of 1.40% decrease rate ($ECO_{1.4}$, *green curve*) ran through a trough between peaks of high ECD group (*black asterisks*) and low ECD group (*red asterisks*). (**B**) High-density group in stage 1 above $ECO_{1.4}$. The age-ECD curve of this group (*red curve*) was close to that of stage 0 (*red dotted curve*), and the calculated decrease rate was 0.56%. (**C**) Low-density group in stage 1 below $ECO_{1.4}$. The age-ECD curve of this group (*red curve*) coincided with $ECO_{2.0}$ (*black dotted curve*), with a decrease rate of 2.00%.

spective, hospital-based review of total 1971 outpatients. In this study, we found a somewhat higher prevalence of guttata cornea than that found in previous reports in Japan. The prevalence of corneal guttae was reported to be 3.7% (1.5% in men, 5.5% in women) in Japan,[17,18] whereas it ranges from approximately 7% up to a remarkable 70.4% in North America, Iceland, and Europe.[1,8,19] In our study, the fact that subjects were hospital-based may have caused a higher prevalence. However, such bias does not have an effect on the validity of the mathematical model derived from the data. The following tendency of prevalence was apparent in our group of subjects: First, females were more predisposed to stages 1, 2, and 3 than were males, and the female ratio increased as stages progressed. Second, the prevalence of FCD was much smaller than stage 1. An increase in the female ratio in progressing stages suggested that sex may have some role not only in the onset but also the progression of the disease. Apparent difference of prevalence between FCD and stage 1 suggest the existence of a patient group in stage 1 that does not progress to corneal edema despite having guttata cornea.

Our model is based on the assumptions that the ECD at 5 years of age is common to all classes and that the decrease rate

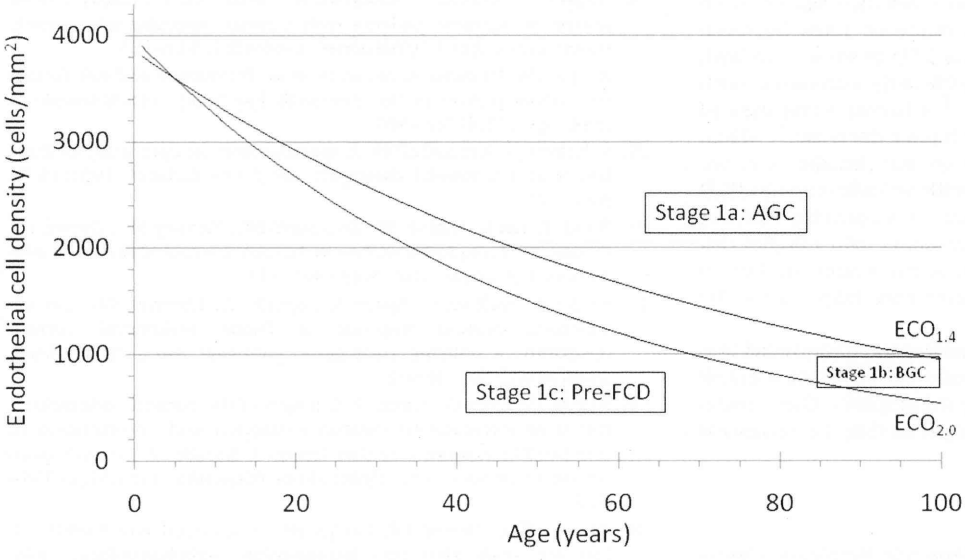

Age (years)		20	30	40	50	60	70	80	90
ECD (cells/mm²)	$ECO_{1.4}$	2918	2537	2205	1917	1667	1449	1260	1095
	$ECO_{2.0}$	2667	2184	1788	1464	1198	981	803	658

Figure 3. Proposed classification of eyes in stage 1 based on $ECO_{1.4}$ and $ECO_{2.0}$. Eyes in stage 1a above $ECO_{1.4}$ were named AGC, which had a decrease rate as low as stage 0. Eyes in stage 1c below $ECO_{2.0}$ had a decrease rate as high as FCD (stages 2 and 3), and therefore, this stage was named pre-FCD. Stage 1b between $ECO_{1.4}$ and $ECO_{2.0}$ was named BGC. The table below the graph shows the coordinates of $ECO_{1.4}$ and $ECO_{2.0}$.

of ECD percentage per year) is constant but with a different value of each class. The use of these assumptions may be a debatable point when discussing the validity of our study. However, the results of our mathematical model show ECD decrease rates that are acceptable when compared with clinical observations. The decrease rate of 0.44% in stage 0 is within the range of values of normal unoperated eyes reported in the previous studies.[10,12–16] Furthermore, since $ECO_{1.4}$ and $ECO_{2.0}$ runs through a clearly defined trough between peaks on the scatterplot, and $ECO_{2.0}$ divided stages 0+1 and stages 2+3 or stage 1 and stages 2+3 with high sensitivity and specificity, we believe our mathematical model for classifying patients with guttae based on ECD decrease rates is adequate for predicting the prognosis.

The $ECO_{1.4}$ and $ECO_{2.0}$ curves based on our mathematical model divided stage 1 into three subgroups, stage 1a, 1b, and 1c. The ECD decrease rate of stage 1a was close to that of stage 0, that is, almost normal. Schnitzer and Krachmer reported on 44 relatives of 12 families with guttata cornea which appeared normal on slit-lamp examination and endothelial cell parameters.[20] These eyes presumably belonged to stage 1a of our classification. In addition, because the distribution of patients of stage 1a was located above $ECO_{1.4}$, the risk of progressing to corneal edema may be as low as stage 0. If a patient was on the curve of a 1.4% decrease rate, the ECD would be 1095 cells/mm^2 even when he was 90 years old. Presumption of low risk of stage 1 is supported by analysis of variance, showing that age-ECD curves of each stage had significant predictability.

It was surprising that the age-ECD curve of the low-density group of stage 1 (stages 1b and 1c) coincided completely with $ECO_{2.0}$. The former was calculated by the least-squares method of the low-density group of stage 1, whereas the latter was obtained from trough between peaks of stages 0 to 3 on scatterplots. This result suggests that the low-density group of stage 1 was located on the border between stage 0 and FCD. Eyes in stage 1c below $ECO_{2.0}$ have a decrease rate as high as FCD, suggesting that these eyes have a risk to progress to FCD, even if there was no corneal edema present. This was the rationale for referring to stage 1c as pre-FCD. Further prospective study of patients in stage 1b and 1c is needed to determine whether stage 1c is a preliminary stage of FCD.

Recently, several pathogenic mechanisms, such as oxidative stress or unfolded protein response, have been reported as causes of FCD.[21,22] The difference in resistance against such stress may cause the difference in decrease rates between stages. Previous reports suggested that ECD of some eyes with guttata cornea did not decrease significantly compared with normal eyes after cataract surgery,[7,23] whereas some eyes in other reports showed a significantly higher decrease.[24] When we adapted data from these reports to our classification, we found that most of the former eyes with no difference in ECD (18/21 eyes) were categorized as stage 1a, suggesting that our classification may be used to identify patients with a higher risk of endothelial damage due to external stress. Future studies on guttata corneas using our classification may help clarify the mechanism of FCD progression.

In conclusion, we assessed distribution and endothelial loss rate of guttata cornea stages 0 to 3 and determined new cutoff curves $ECO_{1.4}$ and $ECO_{2.0}$ by using scatterplots. Our mathematical model is a simple method for predicting the prognosis of patients with guttata cornea.

References

1. Weisenthal RW, Streeten BW, eds. *Posterior Membrane Dystrophies.* London: Elsevier Mosby; 2005.
2. Edelhauser HF, Ubels JL, eds. *The Cornea and the Sclera.* 10th ed. ed. St. Louis: Mosby; 2003.
3. Al-Yousuf N, Mavrikakis I, Mavrikakis E, Daya SM. Penetrating keratoplasty: indications over a 10 year period. *Br J Ophthalmol.* 2004;88(8):998–1001.
4. Dobbins KR, Price FW Jr, Whitson WE. Trends in the indications for penetrating keratoplasty in the midwestern United States. *Cornea.* 2000;19(6):813–816.
5. Kang PC, Klintworth GK, Kim T, et al. Trends in the indications for penetrating keratoplasty. 1980–2001. *Cornea.* 2005;24(7):801–803.
6. Krachmer JH, Purcell JJ Jr, Young CW, Bucher KD. Corneal endothelial dystrophy: a study of 64 families. *Arch Ophthalmol.* 1978; 96(11):2036–2039.
7. Kitagawa K, Fujisawa A, Mizuno T, Sasaki K. Twenty-three cases of primary cornea guttata. *Jpn J Ophthalmol.* 2001;45(1):93–98.
8. Adamis AP, Filatov V, Tripathi BJ, Tripathi RC. Fuchs' endothelial dystrophy of the cornea. *Surv Ophthalmol.* 1993;38(2):149–168.
9. Stocker FW. The endothelium of the cornea and its clinical implications. *Trans Am Ophthalmol Soc.* 1953;51:669–786.
10. Murphy C, Alvarado J, Juster R, Maglio M. Prenatal and postnatal cellularity of the human corneal endothelium: a quantitative histologic study. *Invest Ophthalmol Vis Sci.* 1984;25(3):312–322.
11. Nucci P, Brancato R, Mets MB, Shevell SK. Normal endothelial cell density range in childhood. *Arch Ophthalmol.* 1990;108(2):247–248.
12. Cheng H, Jacobs PM, McPherson K, Noble MJ. Precision of cell density estimates and endothelial cell loss with age. *Arch Ophthalmol.* 1985;103(10):1478–1481.
13. Ambrose VM, Walters RF, Batterbury M, Spalton DJ, McGill JI. Long-term endothelial cell loss and breakdown of the blood-aqueous barrier in cataract surgery. *J Cataract Refract Surg.* 1991; 17(5):622–627.
14. Numa A, Nakamura J, Takashima M, Kani K. Long-term corneal endothelial changes after intraocular lens implantation: anterior vs posterior chamber lenses. *Jpn J Ophthalmol.* 1993;37(1):78–87.
15. Bourne WM, Nelson LR, Hodge DO. Central corneal endothelial cell changes over a ten-year period. *Invest Ophthalmol Vis Sci.* 1997;38(3):779–782.
16. Rao SK, Ranjan Sen P, Fogla R, Gangadharan S, Padmanabhan P, Badrinath SS. Corneal endothelial cell density and morphology in normal Indian eyes. *Cornea.* 2000;19(6):820–823.
17. Kitagawa K, Kojima M, Sasaki H, et al. Prevalence of primary cornea guttata and morphology of corneal endothelium in aging Japanese and Singaporean subjects. *Ophthalmic Res.* 2002;34(3): 135–138.
18. Nagaki Y, Hayasaka S, Kitagawa K, Yamamoto S. Primary cornea guttata in Japanese patients with cataract: specular microscopic observations. *Jpn J Ophthalmol.* 1996;40(4):520–525.
19. Zoega GM, Fujisawa A, Sasaki H, et al. Prevalence and risk factors for cornea guttata in the Reykjavik Eye Study. *Ophthalmology.* 2006 Apr;113(4):565–569.
20. Schnitzer JI, Krachmer JH. A specular microscopic study of families with endothelial dystrophy. *Br J Ophthalmol.* 1981;65(6): 396–400.
21. Buddi R, Lin B, Atilano SR, Zorapapel NC, Kenney MC, Brown DJ. Evidence of oxidative stress in human corneal diseases. *J Histochem Cytochem.* 2002;50(3):341–351.
22. Engler C, Kelliher C, Spitze AR, Speck CL, Eberhart CG, Jun AS. Unfolded protein response in Fuchs endothelial corneal dystrophy: a unifying pathogenic pathway? *Am J Ophthalmol.* 2010;149(2):194–202-e2.
23. Stur M, Grabner G, Dorda W. Changes of the corneal endothelium following intracapsular cataract extraction with implantation of semiflexible anterior chamber lenses. I. Results of the early postoperative period. *Acta Ophthalmol (Copenh).* 1984;62(4):586–594.
24. Bourne WM, Nelson LR, Hodge DO. Continued endothelial cell loss ten years after lens implantation. *Ophthalmology.* 1994; 101(6):1014–1022.

Clinical Significance of Owl Eye Morphologic Features by In Vivo Laser Confocal Microscopy in Patients with Cytomegalovirus Corneal Endotheliitis

AKIRA KOBAYASHI, HIDEAKI YOKOGAWA, TOMOMI HIGASHIDE, KOJI NITTA, AND KAZUHISA SUGIYAMA

• OBJECTIVE: To demonstrate the clinical significance of owl eye morphologic features observed by in vivo laser confocal microscopy in patients with cytomegalovirus (CMV) corneal endotheliitis.

• DESIGN: Observational case series.

• METHODS: PARTICIPANTS: Six eyes of 6 patients (6 men; mean age, 73.3 years) with cytomegalovirus corneal endotheliitis diagnosed by clinical manifestations together with polymerase chain reaction from aqueous humor samples. INTERVENTION: All patients were examined by slit-lamp biomicroscopy and in vivo laser confocal microscopy. MAIN OUTCOME MEASURES: Clinical manifestations were summarized by reviewing medical records. Selected confocal images of corneal layers were evaluated qualitatively for shape and degree of light reflection of abnormal cells and deposits.

• RESULTS: All patients had long histories of anterior uveitis with intraocular pressure elevation, corneal edema with keratic precipitates, and decrease of endothelial cell densities. Coin-shaped lesions were observed by slit lamp only in 1 patient at the first visit and in 2 additional patients at subsequent follow-up. In all patients, confocal microscopy demonstrated reduced subepithelial nerves, subepithelial opacity, increased reflectivity of keratocytes, highly reflective dots, and needle-shaped bodies. Owl eye morphologic features were observed consistently in all patients at the initial visit, and highly reflective round bodies were detected in 5 patients; most notably, these confocal features were reversible after resolution of endotheliitis.

• CONCLUSIONS: Owl eye morphologic features and highly reflective round bodies observed by confocal microscopy may be useful as an adjunct for the noninvasive diagnosis of cytomegalovirus corneal endotheliitis. Reversibility of these features after resolution of endotheliitis may be useful for monitoring the therapeutic effects without multiple anterior chamber tap. (Am J Ophthalmol 2011; xx:xxx. © 2011 by Elsevier Inc. All rights reserved.)

Accepted for publication July 28, 2011.

From the Department of Ophthalmology, Kanazawa University Graduate School of Medical Science, Kanazawa, Japan (A.K., H.Y., T.H., K.S.); and the Department of Ophthalmology, Fukui-ken Saiseikai Hospital, Fukui, Japan (K.N.).

Inquiries to Akira Kobayashi, Department of Ophthalmology, Kanazawa University Graduate School of Medical Science, 13-1 Takara-machi, Kanazawa-shi, Ishikawa-ken 920-8641 Japan; e-mail: kobaya@kenroku.kanazawa-u.ac.jp

CORNEAL ENDOTHELIITIS, CHARACTERIZED BY CORneal edema associated with linear keratic precipitates and endothelial dysfunction,[1] may be caused by herpes simplex virus (HSV),[2] varicella zoster virus (VZV),[3] or other viruses such as mumps.[4] It often leads to irreversible corneal endothelial cell damage and severe visual disturbance. Most recently, cytomegalovirus (CMV) was recognized as a new etiologic factor for corneal endotheliitis.[5] Clinical manifestations of CMV endotheliitis are characterized by linear keratic precipitates associated with multiple coin-shaped lesions and local corneal stromal edema with minimal anterior chamber reactions.[6] The intraocular pressure (IOP) of these patients frequently is increased, and they often are treated with topical or systemic antiglaucoma medication because of the diagnosis of secondary glaucoma of unknown origin.[6] The patients also may have had past histories of several penetrating keratoplasties.[6–8]

In vivo white-light confocal microscopy has been used as a noninvasive technique for the observation of normal and pathologic corneal microstructures at the cellular level in real time.[9–13] Most recently, new-generation scanning laser in vivo confocal microscopy (Heidelberg Retina Tomograph 2 Rostock Cornea Module [HRT 2-RCM]; Heidelberg Engineering GmbH, Dossenheim, Germany) has become available.[14–16] This new device provides high-definition histologic-like images of corneal microstructures in vivo, with an axial resolution of approximately 4 μm and improved resolution compared with conventional white-light confocal microscopes (for example, 10 μm axial optical resolution with ConfoScan 2 [Nidek Technologies, Vigonza, Italy]).[17,18] Previously, Shiraishi and associates demonstrated large corneal endothelial cells with an area of high reflection in the nucleus surrounded by a halo of low reflection in a single patient with CMV corneal endotheliitis using the HRT 2-RCM.[19] The authors suggest that these owl eye morphologic features in the corneal endothelium may be characteristic of CMV endotheliitis. A small number of case reports also have suggested an association of owl eye morphologic features in the corneal endothelium and CMV corneal endotheliitis.[6,8]

In this article, we report clinical manifestations in 6 Japanese patients with polymerase chain reaction (PCR)-proven CMV corneal endotheliitis and the re-

0002-9394/$36.00
doi:10.1016/j.ajo.2011.07.026

TABLE. Clinical Data and Slit-Lamp Biomicroscopic Findings of 6 Patients with Cytomegalovirus Corneal Endotheliitis

Case No.	Gender/ Age (y)	Age (y)	Affected Eye	History of Ocular Disease and Duration (mos)	Slit-Lamp Findings	Endothelial Cell Density (cells/mm^2)
1	M	77	Left	Anterior uveitis, secondary glaucoma (72)	Corneal edema, pigmented KPs (coin-shaped lesions during follow-up), AC cell	692
2	M	75	Left	Anterior uveitis, secondary glaucoma (24), diagnosed as Posner- Schlossman syndrome	Corneal edema, pigmented KPs, coin-shaped lesions, AC cell	1730
3	M	63	Right	Anterior uveitis, secondary glaucoma (108), diagnosed as Posner-Schlossman syndrome	Corneal edema, pigmented KPs (coin-shaped lesions during follow-up), AC cell+, iris atrophy	1677
4	M	83	Right	Anterior uveitis, secondary glaucoma (60)	Corneal edema, Pigmented KPs AC cell+, fibrin+	645
5	M	56	Left	Anterior uveitis, secondary glaucoma, (144), diagnosed as Posner-Schlossman syndrome	Corneal edema, pigmented KPs, AC cell+, iris atrophy	<1000
6	M	86	Left	Anterior uveitis, secondary glaucoma (96), diagnosed as Posner- Schlossman syndrome	Corneal edema, pigmented KPs, AC cell, depigmented iris	550

AC = anterior chamber; CMV = cytomegalovirus; DNA = deoxyribonucleic acid; DM = diabetes mellitus; Dx = diamox; F = female; KPs = keratic precipitates; M = male; PCR = polymerase chain reaction.

Continued on next page

sults of detailed investigations of in vivo corneal microstructures of all cell layers with laser scanning confocal microscopy using the HRT 2-RCM. The diagnostic value and usefulness of monitoring the therapeutic effects of this device in CMV corneal endotheliitis also are described.

METHODS

THE STUDY POPULATION CONSISTED OF 6 EYES OF 6 CONsecutive patients (6 men; mean, 73.3 years), whose active CMV corneal endotheliitis was diagnosed and treated between April 2010 and March 2011 at the Department of Ophthalmology, Kanazawa University Hospital, Kanazawa, Japan (Patients 1 through 5), or the Department of Ophthalmology, Fukui-ken Saiseikai Hospital, Fukui, Japan (Patient 6; Table). The clinical diagnosis was performed based on slit-lamp findings of active corneal endotheliitis (such as corneal edema and keratic precipitates) and the detection of CMV by PCR assay in the aqueous humor from the affected eye. HSV, VZV, Epstein-Barr virus, human herpes virus 6, and human herpes virus 7 DNA were not detected. Clinical manifestations of the patients were reviewed retrospectively, with special attention paid to slit-lamp findings, IOP measurements, and corneal endothelial cell density. Also, responses to antiviral treatment were evaluated.

• IN VIVO LASER CONFOCAL MICROSCOPY: Before examination, written informed consent was obtained from all subjects after explaining the nature and possible consequences of this study, such as superficial punctate keratopathy. After applying a large drop of contact gel (Comfort Gel ophthalmic ointment; Bausch & Lomb GmbH, Berlin, Germany) on the front surface of the microscope lens and ensuring that no air bubbles had formed, a Tomo-Cap (Heidelberg Engineering GmbH, Dossenheim, Germany) was mounted on the holder to cover the microscope lens. The central and affected areas of the cornea then were examined layer by layer using the HRT 2-RCM. The HRT 2-RCM uses a ×60 water-immersion objective lens (Olympus Europa GmbH, Hamburg, Germany) and uses a 670-nm diode laser as the light source with a 400-μm^2 area of observation.

RESULTS

• CLINICAL MANIFESTATIONS: The Table summarizes the clinical manifestations for 6 eyes of 6 patients. The mean follow-up period for all patients was 4.2 ± 2.5

TABLE. Clinical Data and Slit-Lamp Biomicroscopic Findings of 6 Patients with Cytomegalovirus Corneal Endotheliitis *(Continued)*

Systemic Disease	Intraocular Pressure (mm Hg) (No. Antiglaucoma Eye Drops)	Visual Acuity before/after Treatment	CMV DNA by PCR of Aqueous Humor	Treatment	Clinical Outcomes (Follow-up Period after CMV Detection, mos)
DM, mixed connective tissue disease (oral prednisolone 2.5 mg/day)	18 (1)	20/25/20/25	Positive	Systemic ganciclovir 10 mg/kg daily × 7 days, 0.5% ganciclovir, 8 times daily, 0.1% betamethasone, 4 times daily	Clear cornea (8)
Lung cancer (treated)	25 (3+Dx)	20/40/20/40	Positive	0.5% ganciclovir 8 times daily, 0.1% betamethasone 4 times daily	Clear cornea (5)
Hyperlipidemia, fatty liver	24 (3+Dx)	20/25/20/25	Positive	Systemic ganciclovir 10 mg/kg daily × 7 days, 0.5% ganciclovir 8 times daily, 0.1% betamethasone 4 times daily, cataract surgery for secondary cataract	Edema reduction (5)
Essential thrombocythemia	26 (2)	20/100/20/40	Positive	0.5% ganciclovir 8 times daily, 0.1% betamethasone 4 times daily	Clear cornea (4)
DM	15 (4)	20/100/12/40	Positive	Systemic ganciclovir 1800 mg daily × 12 days, 0.5% ganciclovir 8 times daily, 0.1% betamethasone 4 times daily	Edema reduction (2)
Hypertension	43 (3+Dx)	20/22/20/16	Positive	Systemic ganciclovir 10 mg/kg daily × 14 days, 0.5% ganciclovir 8 times daily, 0.1% betamethasone 4 times daily	Edema reduction (1)

months (range, 1 to 8 months). All patients were male (6/6; 100%) and had long histories (more than 2 years) of anterior uveitis (6/6; 100%) and IOP elevation of unknown origin (6/6; 100%) that was treated by corticosteroids and antiglaucoma agents (duration, 24 to 144 months; mean ± standard deviation, 84.0 ± 41.6 months). All patients had corneal edema (6/6; 100%) and pigmented keratic precipitates (6/6; 100%). Three patients had mild anterior chamber reaction (Patients 3 through 5; 50%), and the remaining 3 patients had no anterior chamber reaction. Iris atrophy was observed in 3 patients (Patients 3, 5, and 6; 3/6; 50%). Three patients experienced strong iridocyclitis with fibrin reaction after cataract surgery (3/4; 75%); the surgery was performed before the diagnosis of CMV endotheliitis in 1 patient and after the treatment of CMV endotheliitis in 2 patients. A tentative diagnosis of Posner-Schlossman syndrome was made in 4 patients (Patients 2, 3, 5, and 6; 4/6; 66.7%), and 5 patients (5/6, 83.3%) initially were referred to our glaucoma service. Severe glaucomatous visual field defects were observed in 2 patients (2/6; 33.3%).

Coin-shaped lesions were observed only in Patient 2 at the first visit. At subsequent follow-up visits, 2 additional patients had coin-shaped lesions (Patients 1 and 3; total, 3/6; 50%: Figure 1). The coin-shaped lesions were not detectable in the remaining 3 patients (Patients 4 through 6) throughout the follow-up period. Endothelial cell density (ECD) was decreased in all eyes (6/6; 100%); 4 patients (Patients 1, 4, 5, and 6) had an ECD of less than 1000/mm^2, and the remaining 2 patients had an ECD of less than 2000/mm^2. Patients 1 and 5 had diabetes mellitus, and Patient 1 also had mixed connective tissue disease treated with oral prednisolone 2.5 mg/day. The aqueous humor samples of all eyes contained CMV DNA (6/6; 100%), but not HSV, VZV, Epstein-Barr virus, human herpes virus 6, or human herpes virus 7 DNA. All patients were treated with topical 0.5% ganciclovir (8 times daily) and 0.1% betamethasone (4 times daily). In addition, all patients (except Patients 2 and 4) were administrated intravenous ganciclovir 10 mg/kg daily for 7 days based on the severity of clinical manifestations. After 1 to 2 months of treatment, corneal edema, keratic precipitates (KPs), and IOP were improved in all patients. In Patients 1 and 3, CMV DNA was not detected by PCR in aqueous humor samples after treatment. CMV DNA was not tested again in the remaining patients.

• IN VIVO LASER CONFOCAL MICROSCOPY: In vivo laser confocal microscopy demonstrated normal epithelial layers in 4 patients (Patients 1, 2, 4, and 5; 66.7%) and slightly increased cell body size with higher intensity indicative of epithelial edema in 2 patients (Patients 3 and 6; 33.3%: Figure 2, Top right). A few subepithelial nerves were detected in 2 patients (Patients 3 and 4; 33.3%; Figure 2,

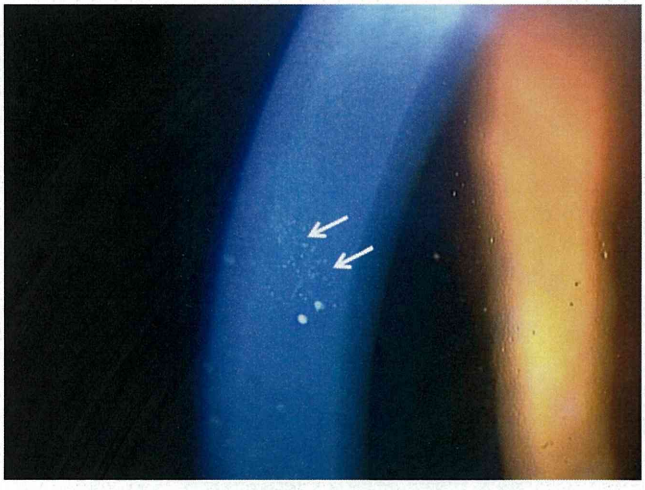

FIGURE 1. Coin-shaped lesion identified by slit lamp in a patient with cytomegalovirus corneal endotheliitis. Coin-shaped lesion was observed in Patient 1 during the follow-up period (arrows). This was not noted at the initial visit.

Second row left), but no subepithelial nerves were detected in the remaining 4 patients (Patients 1, 2, 5, and 6; 66.7%; Figure 3, Second row left; Figure 4, Second row left). Stromal nerves were detected in 2 patients (Patients 2 and 3; 33.3%). Subepithelial opacity, increased reflectivity of keratocytes, highly reflective dots, and needle-shaped bodies were observed uniformly in all patients (6/6; 100%; Figure 3, Second row center and Second row right; Figure 4, Second row center and Second row right; Figure 2, Second row center and Second row right). The most characteristic feature was large cells whose nuclei had a high reflection area surrounded by a halo of low reflection (owl eye morphologic features), and these were observed in the corneal endothelial cell layer in all eyes (6/6; 100%; Figure 2, Bottom left and Bottom center, Figure 3, Third row left, Third row center, Third row right, and Bottom center; Figure 4, Bottom left and Bottom center). In contrast, owl eye morphologic features were not detected by noncontact specular microscopy in any of the patients (data not shown). Highly reflective round bodies on the surface of the endothelial cell layer also were detectable in 5 patients (Patients 1 through 3, 5, and 6; 83.3%; Figure 2, Bottom right, Figure 3, Bottom left, Bottom center, Bottom right; Figure 4, Bottom right). These owl eye cells and highly reflective round bodies disappeared in all patients after treatment. Subepithelial and stromal nerves were visible in all patients after resolution of the CMV endotheliitis.

• CASE REPORT: A 75-year-old man (Case 2) began to experience recurrent episodes of anterior uveitis of unknown origin and IOP elevation to 40 mm Hg in his left eye in June 2008. He was diagnosed with bilateral glaucoma and Posner-Schlossman syndrome and was treated with topical corticosteroids and antiglaucoma agents. He was referred to the glaucoma service at our hospital in June 2010 for poor IOP control. He had a history of lung cancer (treated). At the initial visit, his BCVA was 20/40 in the left eye. His left cornea had localized corneal edema, pigmented KPs in the lower cornea, and coin-shaped lesions with minimal anterior chamber reaction (Figure 4, Top left and Top center). Iris atrophy was not noted. ECD was 1730 cells/mm^2 in his left eye and 2785 cells/mm^2 in his right eye. IOP was 9 mm Hg (right) and 25 mm Hg (left) with antiglaucoma agents (topical latanoprost, dorzolamide, bunazosin, and oral acetazolamide). Bilateral glaucomatous optic neuropathy was observed, but CMV retinitis was not observed by fundus examination. Owl eye morphologic features were observed by HRT2-RCM examination in his left eye (Figure 4, Bottom left and Bottom center). PCR analysis of aqueous humor samples for the left eye detected CMV, but not HSV, VZV, Epstein-Barr virus, human herpes virus 6, or human herpes virus 7 DNA. In August 2010, based on the diagnosis of CMV corneal endotheliitis in the left eye, topical 0.5% ganciclovir was applied 8 times daily, and 0.1% betamethasone was applied 4 times daily, but he was not treated with systemic ganciclovir. The corneal edema disappeared rapidly, and the KPs and IOP improved gradually. In November 2010, the owl eye morphologic features had disappeared in the endothelial layer by HRT2-RCM examination. In January 2011, the left eye IOP was reduced to 11 mm Hg under a single antiglaucomatous agent (topical dorzolamide only).

DISCUSSION

HEREIN, WE REPORT THE CLINICAL MANIFESTATIONS together with detailed in vivo laser confocal microscopic findings of all corneal cell layers in 6 Japanese patients with PCR-proven CMV corneal endotheliitis. To the best of the authors' knowledge, this is the largest series of confocal microscopic analyses of CMV corneal endotheliitis. The main highlight of the case series is the supportive diagnostic value of owl eye morphologic features by confocal microscopy. Most notably, we found that these confocal features are reversible after resolution of corneal endotheliitis.

In vivo laser confocal microscopy demonstrated epithelial edema in 2 patients (2/6; 33.3%), reduced or nondetectable subepithelial nerves in all patients (100%; 6/6), reduced stromal nerves in 2 patients (2/6; 33.3%), subepithelial opacity in all patients (6/6; 100%), increased reflectivity of keratocytes in all patients (6/6; 100%), and highly reflective dots and needle-shaped bodies in all patients (6/6; 100%). These confocal characteristics most likely were the result of common pathologic changes seen in edematous cornea caused by endothelial dysfunction, corneal stromal inflammation, or both.[16,20–23] However,

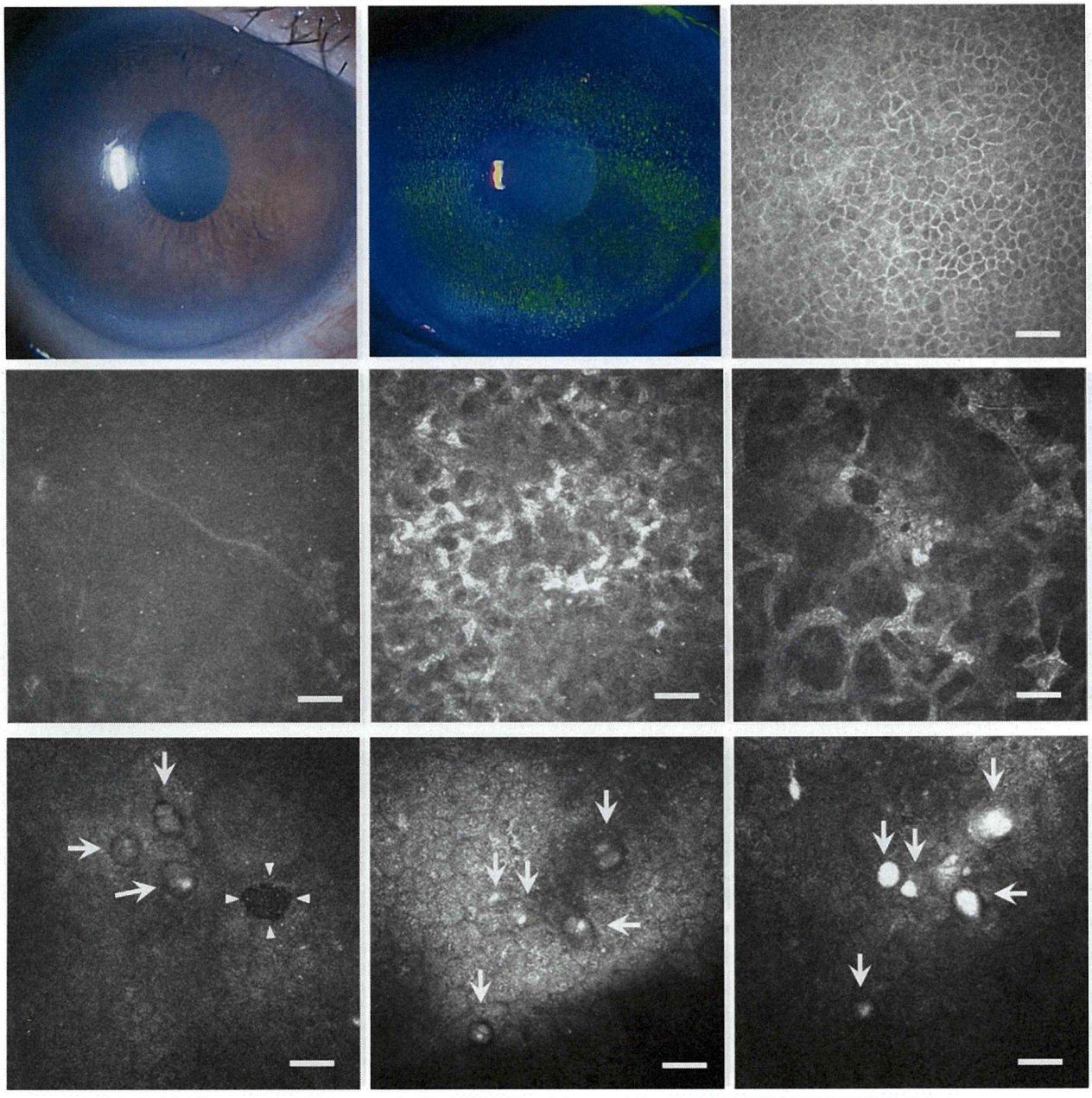

FIGURE 2. Slit-lamp photographs and laser confocal microscopy scans from a patient with cytomegalovirus corneal endotheliitis (Patient 3). (Top left) Slit-lamp photograph of the right cornea of Patient 3 at an initial visit to the hospital. Brown pigmented keratic precipitates were seen in the lower part of the cornea. (Top middle) Sectorial edemas from periphery to mid periphery were detected under fluorescein staining. (Top right) Epithelial basal cell layer in the center of the cornea showed slight edema by Heidelberg Retina Tomograph 2 Rostock Cornea Module (HRT 2-RCM). Bar = 50 μm. (Second row left) Bowman layer with highly reflective tiny dots. Nerve density was reduced. (Second row middle) Subepithelial opacity with increased reflectivity of keratocytes was observed. (Second row right) Highly reflective activated keratocytes were seen. (Bottom left and middle) Owl eye morphologic features were detectable by HRT 2-RCM (arrows). Endothelial cell density was 1677 cells/mm^2. (Bottom right) Sequential image of Bottom row middle, 8 μm forward toward the anterior chamber. Highly reflective round bodies, presumably the identical cell of owl eye morphologic features seen in Bottom row middle were noted (arrows).

the precise origin and significance of these pathologic changes remain unclear. It should be noted that subepithelial and stromal nerves were reversible in all cases after resolution of the CMV endotheliitis.

The most characteristic feature was large cells, whose nuclei had a high reflection area surrounded by a halo of low reflection (owl eye morphologic features), which were observed in the corneal endothelial cell layer by HRT2-

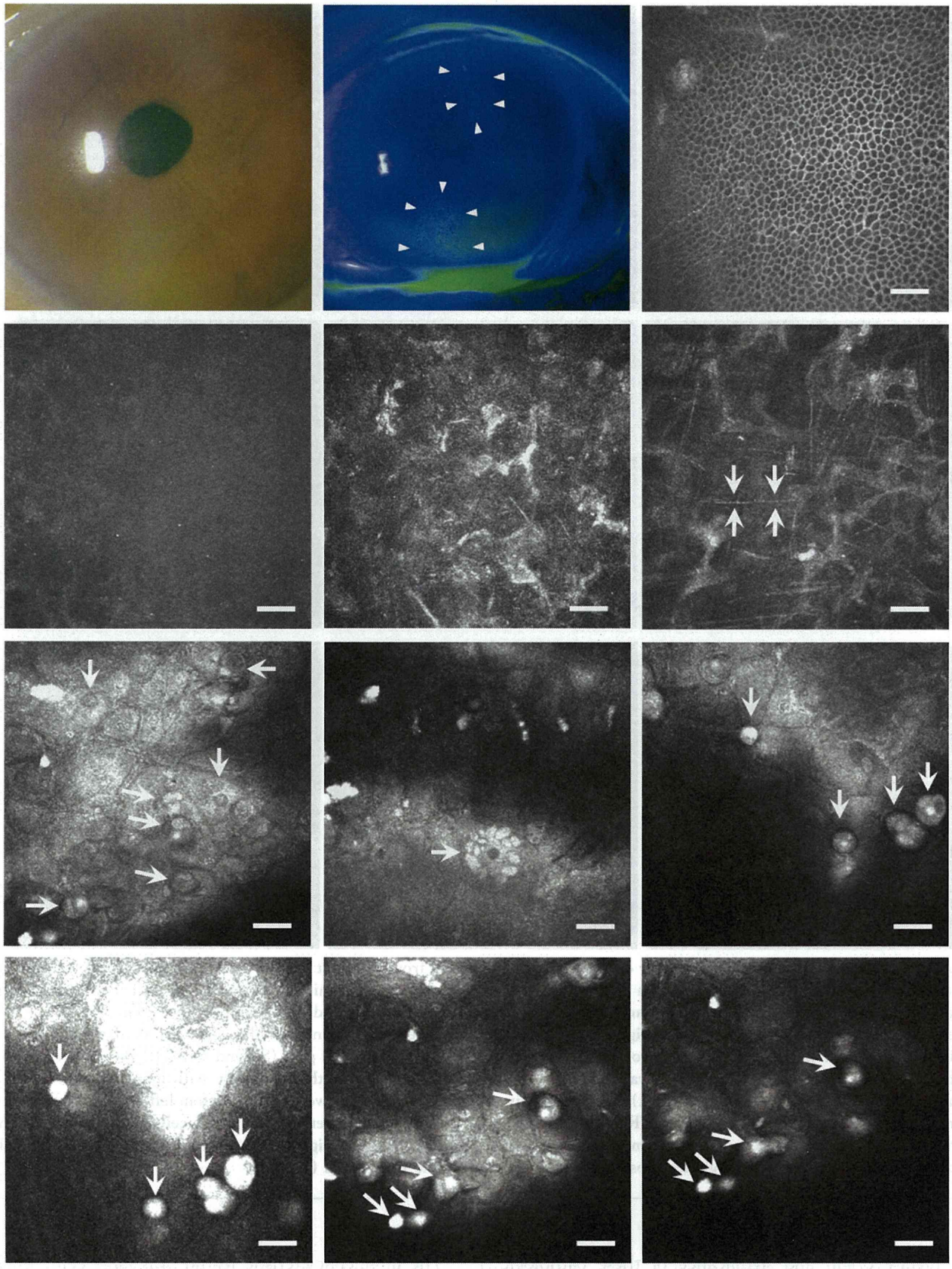

FIGURE 3. Slit-lamp photographs and laser confocal microscopy scans from a patient with cytomegalovirus corneal endotheliitis (Patient 1). (Top left and center) Slit-lamp photographs of the left cornea of Patient 1 at the initial visit to the hospital. Faint keratic

RCM in all eyes at the initial visit (6/6; 100%). This indicates the potential usefulness of visualizing owl eye morphologic features in the diagnosis of CMV corneal endotheliitis. Owl eye cells typically are seen at autopsy or in biopsy specimens from the kidneys, lungs, and other organs in cases of congenital or acquired CMV infection.[24] Shiraishi and associates were the first to report the owl eye morphologic features in a single case of CMV corneal endotheliitis using HRT2-RCM.[19] In their study, owl eye morphologic features in the corneal endothelial cell layer observed by in vivo laser confocal microscopy were described as "a group of large cells whose nuclei have a high reflection area surrounded by a halo of low reflection."[19] Subsequently, 2 case reports showed the presence of owl eye morphologic features by in vivo laser confocal microscopy in CMV corneal endotheliitis: Koizumi and associates reported an owl eye morphologic features in 1 patient, and Wang and associates reported 1 patient with owl eye morphologic features after penetrating keratoplasty.[6,8] In this study, we reported 6 cases of PCR-proven CMV corneal endotheliitis, and all cases (100%) demonstrated owl eye morphologic features by HRT2-RCM. Furthermore, the owl eye morphologic features disappeared after treatment in all patients. Thus, HRT2-RCM may be useful not only for diagnosing CMV corneal endotheliitis, but also for monitoring the therapeutic effects of systemic or topical antiviral drugs. Moreover, this may provide information regarding the timing for discontinuing medications in a noninvasive manner compared with PCR testing, which requires an anterior chamber tap. It should be noted that the owl eye morphologic features were not detected by noncontact specular microscopy in any of the patients. One explanation of this discrepancy of observation between the 2 diagnostic methods may be the difference of observational area. In specular microscopy, only the central endothelium is visualized. In contrast, by confocal microscopy, scanning a wide area of endothelium is possible, enabling rapid detection of owl eye morphologic features. Another important explanation is the difference of principals of visualizing the endothelium. In specular microscopy, specular reflection can be obtained only when the endothelium is smooth. Also, specular microscopy visualizes only the surface of the endothelial cells. In contrast, by confocal microscopy, all cell layers can be visualized with high resolution and pathologic endothelium, such as guttae seen in Fuchs dystrophy, can be observed clearly. Therefore, confocal microscopy may be a reasonable device to visualize the owl eye morphologic features, because the features are a characteristic light reflection inside the endothelial cells, which probably correspond to the intranuclear inclusion body.

One notable finding from our in vivo laser confocal microscopic study is that highly reflective round bodies with a diameter of 10 to 30 μm were observed on the surface of the corneal endothelium in 5 patients (5/6; 83.3%). These deposits did not look like the images of KPs usually seen in various kinds of uveitis.[25,26] On careful examination using consecutive images around the level of the endothelial cell layer, we noted that these deposits were localized on the surface of the endothelial cells and were related to the owl eye morphologic features (Figure 2, Bottom row middle and right, Figure 3, Third row right, Bottom row). We assumed that the highly reflective round bodies were CMV infected and were necrotic endothelial cells that protruded or had fallen off toward the anterior chamber. The fact that highly reflective round bodies disappeared after treatment in all patients also suggests that these are closely related to the owl eye morphologic features.

Koizumi and associates found coin-shaped lesions by slit-lamp biomicroscopy in all patients (8/8; 100%) and suggested that the lesions are a characteristic sign of CMV corneal endotheliitis.[6] However, we detected coin-shaped lesions in only 1 patient (16.7%) at the first visit. At subsequent follow-up visits, 2 additional patients had coin-shaped lesions (Figure 1; total, 3/6; 50%). The coin-shaped lesions were not detectable in the remaining 3 patients throughout the follow-up visits. Considering that we could visualize owl eye morphologic features in all patients (6/6; 100%), the presence of not only coin-shaped lesions by slit-lamp biomicroscopy, but also of owl eye morphologic features by HRT2-RCM may be useful as an adjunct method for the noninvasive diagnosis of CMV corneal endotheliitis. For example, owl eye morphologic features may indicate that ganciclovir treatment should be initiated soon after the confocal examination under ten-

precipitates in the peripheral cornea were observed. Sectorial edemas from the periphery to the center were detected under fluorescein staining (arrowheads). (Top right) Epithelial basal cell layer in the center of the cornea demonstrating normal results by Heidelberg Retina Tomograph 2 Rostock Cornea Module (HRT 2-RCM). Bar = 50 μm. (Second row left) Seemingly normal Bowman layer with minimal highly reflective tiny dots. Nerves were not detectable. (Second row middle) Subepithelial opacity with increased reflectivity of keratocytes was observed. (Second row right) Highly reflective dots and needle-shaped bodies (arrows) were noted. (Third row left) HRT 2-RCM identified large endothelial cells whose nuclei had a high reflection area surrounded by a halo of low reflection, which resembled an owl eye (arrows). Endothelial cell density was 692 cells/mm^2. (Third row middle) Multiple intranuclear inclusion bodies in a cartwheel arrangement were seen in large cells (arrow). (Third row right) Further owl eye morphologic features were noted during the subsequent follow-up visit (arrows). (Bottom left) Sequential image of Third row right, 4 μm forward from the anterior chamber. Highly reflective round bodies were noted, which presumably show necrotic and protruded owl eye cells identified in Third row right (arrows). (Bottom middle) Owl eye morphologic features in a different location (arrows). (Bottom right) Sequential image of Bottom middle, 6 μm forward toward the anterior chamber. Highly reflective round bodies, presumably the identical cell of owl eye morphologic features seen in the Bottom middle were noted (arrows).

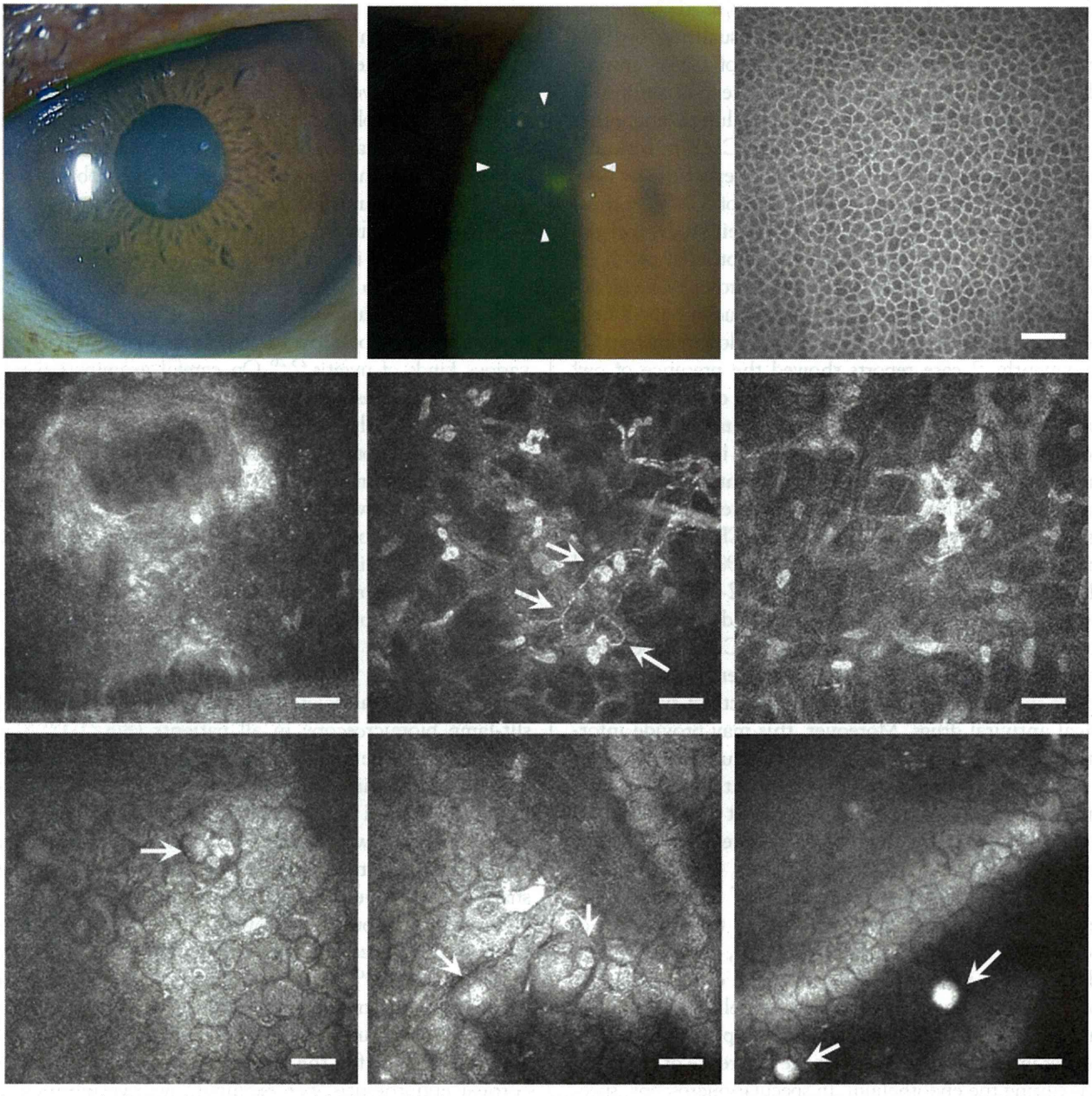

FIGURE 4. Slit-lamp photographs and laser confocal microscopy scans from a patient with cytomegalovirus corneal endotheliitis (Patient 2). (Top left) Slit-lamp photograph of the left cornea of Patient 2 at an initial visit to the hospital. (Top center) Coin-shaped lesions and disciform edema were observed in the upper temporal region (arrowheads). (Top right) Epithelial basal cell layer in the center of the cornea demonstrating normal results by Heidelberg Retina Tomograph 2 Rostock Cornea Module (HRT 2-RCM). Bar = 50 μm. (Second row left) Increased intensity of Bowman layer with highly reflective tiny dots were observed. (Second row middle) Aberrant shape of subepithelial nerves was observed (arrows). (Second row right) Subepithelial opacity with increased reflectivity of keratocytes and highly reflective needle-shaped bodies were noted. (Bottom middle and left) Owl eye morphologic features were detectable by HRT 2-RCM (arrows). Endothelial cell density was 1730 cells/mm^2. (Bottom right) Highly reflective round bodies were noted (arrows).

tative clinical diagnosis of CMV corneal endotheliitis, which may prevent further endothelial cell loss that may happen while waiting for the PCR results. However, one limitation of confocal microscopic examination is that the device may not be useful for patients with severe corneal stromal edema, because this may prevent visualization of the corneal endothelium layer.

We hypothesized that aggregates of highly reflective round bodies visualized by HRT2-RCM may correspond to the coin-shaped lesions observed by slit-lamp biomicroscopy.

That is, the coin-shaped lesions may correspond to necrotic and aggregated corneal endothelial cells that are infected with CMV. The fact that the owl eye morphologic features are visualized better around the area of coin-shaped lesions, but are not seen uniformly in the endothelial cell layer (unpublished observation), also may support this hypothesis.

In conclusion, in vivo laser confocal microscopy is capable of identifying characteristic corneal microstructural changes related to CMV corneal endotheliitis. Specifically, owl eye morphologic features and highly reflective round bodies may be useful adjuncts for the noninvasive diagnosis of CMV corneal endotheliitis. Additionally, HRT2-RCM may be useful for monitoring the therapeutic effects of systemic and topical antiviral drugs and may provide information regarding the timing for discontinuing medications without multiple anterior chamber tap. Further studies using a large number of patients and including other types of endothelial diseases are required to elucidate fully the clinical significance of owl eye morphologic features in CMV endotheliitis.

PUBLICATION OF THIS ARTICLE WAS SUPPORTED BY GRANT 10103447 FROM THE INTRACTABLE DISEASE TREATMENT Research Program; the Ministry of Health, Labour and Welfare, Tokyo, Japan; and Grant-in-Aid for Scientific Research 22591934 from Kakenhi, Tokyo, Japan. The sponsors or funding organizations had no role in the design or conduct of this research. The corresponding investigator (A.K.) has full access to all data in the study and takes responsibility for the integrity of the data and accuracy of the data analysis. The authors indicate no financial conflict of interest. Involved in Design (A.K.) and conduct (H.Y., A.K., K.N.) of study; Collection, management, analysis, and interpretation of the data (H.Y., A.K.); and Preparation, review, or approval of manuscript (T.H., K.S.). This prospective study was approved by the Ethical Committee of Kanazawa University Graduate School of Medical Science and followed the tenets of the Declaration of Helsinki.

REFERENCES

1. Khodadoust AA, Attarzadeh A. Presumed autoimmune corneal endotheliopathy. Am J Ophthalmol 1982;93(6):718–722.
2. Ohashi Y, Yamamoto S, Nishida K, et al. Demonstration of herpes simplex virus DNA in idiopathic corneal endotheliopathy. Am J Ophthalmol 1991;112(4):419–423.
3. Maudgal PC, Missotten L, De Clercq E, Descamps J. Varicella-zoster virus in the human corneal endothelium: a case report. Bull Soc Belge Ophthalmol 1980;190:71–86.
4. Singh K, Sodhi PK. Mumps-induced corneal endotheliitis Cornea 2004;23(4):400–402.
5. Koizumi N, Yamasaki K, Kawasaki S, et al. Cytomegalovirus in aqueous humor from an eye with corneal endotheliitis. Am J Ophthalmol 2006;141(3):564–565.
6. Koizumi N, Suzuki T, Uno T, et al. Cytomegalovirus as an etiologic factor in corneal endotheliitis. Ophthalmology 2008;115(2):292–297.
7. Sonoyama H, Araki-Sasaki K, Osakabe Y, et al. Detection of cytomegalovirus DNA from cytomegalovirus corneal endotheliitis after penetrating keratoplasty. Cornea 2010;29(6):683–685.
8. Wang SC, Tsai IL, Lin HC, et al. Recurrent cytomegalovirus corneal endotheliitis after penetrating keratoplasty. Eur J Ophthalmol 2010;20(2):457–459.
9. Cavanagh HD, Petroll WM, Alizadeh H, et al. Clinical and diagnostic use of in vivo confocal microscopy in patients with corneal disease. Ophthalmology 1993;100(10):1444–1454.
10. Bohnke M, Masters BR. Confocal microscopy of the cornea. Prog Retin Eye Res 1999;18(5):553–628.
11. Kaufman SC, Musch DC, Belin MW, et al. Confocal microscopy: a report by the American Academy of Ophthalmology. Ophthalmology 2004;111(7):396–406.
12. Kobayashi A, Sugiyama K. In vivo corneal confocal microscopic findings of palisades of Vogt and its underlying limbal stroma. Cornea 2005;24(4):435–437.
13. Kobayashi A, Sugiyama K, Huang AJ. In vivo confocal microscopy in patients with central cloudy dystrophy of Francois. Arch Ophthalmol 2004;122(11):1676–1679.
14. Zhivov A, Stachs O, Kraak R, et al. In vivo confocal microscopy of the ocular surface. Ocul Surf 2006;4(2):81–93.
15. Kobayashi A, Yokogawa H, Sugiyama K. In vivo laser confocal microscopy of Bowman's layer of the cornea. Ophthalmology 2006;113(12):2203–2208.
16. Kobayashi A, Sugiyama K. In vivo laser confocal microscopy findings for Bowman's layer dystrophies (Thiel-Behnke and Reis-Bücklers corneal dystrophies). Ophthalmology 2007;114(1):69–75.
17. Heidelberg Engineering. Heidelberg Retina Tomograph 2 (Rostock Cornea Module) Operating Instructions of software version 1.1. Dossenheim, Germany: Heidelberg Engineering; 2004.
18. Nidek Technologies. Confoscan 2: operator's manual. Vigonza, Italy: Nidek Technologies; 2001.
19. Shiraishi A, Hara Y, Takahashi M, et al. Demonstration of "owl's eye" morphology by confocal microscopy in a patient with presumed cytomegalovirus corneal endotheliitis. Am J Ophthalmol 2007;143(4):715–717.
20. Kobayashi A, Mawatari Y, Yokogawa H, Sugiyama K. In vivo laser confocal microscopy after Descemet stripping with automated endothelial keratoplasty. Am J Ophthalmol 2008;145(6):977–985.
21. Kobayashi A, Yokogawa H, Sugiyama K. In vivo laser confocal microscopy after non-Descemet's stripping automated endothelial keratoplasty. Ophthalmology 2009;116(7):1306–1313.
22. Efron N. Contact lens-induced changes in the anterior eye as observed in vivo with the confocal microscope. Prog Retin Eye Res 2007;26(4):398–436.
23. Kobayashi A, Maeda A, Sugiyama K. In-vivo confocal microscopy in the acute phase of corneal inflammation. Ophthalmic Surg Lasers Imaging 2003;34(5):433–436.
24. Herriot R, Gray ES. Images in clinical medicine: owl's-eye cells. N Engl J Med 1994;331(10):649.
25. Wertheim MS, Mathers WD, Planck SJ, et al. In vivo confocal microscopy of keratic precipitates. Arch Ophthalmol 2004;122(12):1773–1781.
26. Mocan MC, Kadayifcilar S, Irkec M. Keratic precipitate morphology in uveitic syndromes including Behçet's disease as evaluated with in vivo confocal microscopy. Eye 2009;23(5):1221–1227.

Jpn J Ophthalmol 2011;55:98–102
DOI 10.1007/s10384-010-0916-8

CLINICAL INVESTIGATION

Intraocular Pressure After Descemet's Stripping and Non-Descemet's Stripping Automated Endothelial Keratoplasty

Yoshiro Mawatari, Akira Kobayashi, Hideaki Yokogawa, and Kazuhisa Sugiyama

Department of Ophthalmology, Kanazawa University Graduate School of Medical Science, Kanazawa, Japan

Abstract

Purpose: To evaluate the effect on intraocular pressure (IOP) of increased corneal thickness after Descemet's stripping automated endothelial keratoplasty (DSAEK) and of non-Descemet's stripping automated endothelial keratoplasty (nDSAEK) as measured by four different techniques.

Methods: Twenty-four eyes (22 patients; mean age, 74.0 years) with successful DSAEK (11 eyes) or nDSAEK (13 eyes) treatment at least 3 months prior to testing were enrolled. IOP was measured with Goldmann applanation tonometry (GAT), dynamic contour tonometry (DCT), pneumatonometry, and Tono-Pen XL (Tonopen). Central corneal thickness (CCT) was measured by ultrasonic pachymetry. These data were used for statistical analysis.

Results: Mean IOP measured by GAT, DCT, pneumatonometry, and Tonopen was 14.4, 13.9, 11.2, and 13.2 mmHg, respectively, in the DSAEK group; and 15.0, 14.4, 12.5, and 14.4 mmHg, respectively, in the nDSAEK group. Correlations between IOP and CCT were not statistically significant in either group. Pressure measured by pneumatonometry was significantly and consistently lower than that obtained by the other three methods.

Conclusion: For both DSAEK and nDSAEK, IOP readings by the four tonometers seem to be unrelated to artificially thickened corneas. **Jpn J Ophthalmol** 2011;55:98–102 © Japanese Ophthalmological Society 2011

Keywords: DSAEK, endothelial keratoplasty, intraocular pressure, nDSAEK

Introduction

Over the past several years, new surgical techniques have been reported for bullous keratopathy that replace only the dysfunctional posterior portion of the cornea through a scleral pocket incision.[1–5] These techniques completely eliminate surface corneal incisions and sutures, maintain much of the cornea's structural integrity, and induce minimal refractive changes, suggesting distinct advantages over standard penetrating keratoplasty. Recently, preparation of donor tissue for this type of procedure, termed endothelial keratoplasty, has been made easier with the utilization of an automated microkeratome. The enhanced surgical procedure with the automated microkeratome is known as Descemet's stripping automated endothelial keratoplasty (DSAEK).[4,6] Recently, we reported a successful modification of DSAEK without Descemet's membrane peeling for bullous keratopathies secondary to Argon laser iridotomy; we termed the modified procedure non-Descemet's stripping automated endothelial keratoplasty (nDSAEK).[7,8]

After both DSAEK and nDSAEK surgery, corneal thickness inevitably increases owing to the addition of the

Received: May 10, 2010 / Accepted: November 5, 2010
Correspondence and reprint requests to: Akira Kobayashi, Department of Ophthalmology, Kanazawa University Graduate School of Medical Science, 13-1 Takara-machi, Kanazawa, Ishikawa 920-8641, Japan
e-mail: kobaya@kenroku.kanazawa-u.ac.jp

Originally presented at the Association for Research in Vision and Ophthalmology Annual Meeting, 2 May 2010, Fort Lauderdale, Florida, USA.

donor graft. Therefore, there is a possibility that intraocular pressure (IOP) measurement methods dependent on normal corneal thickness, such as Goldmann applanation tonometry (GAT), may produce less accurate readings.

The purpose of the current study was to evaluate the effect of both post-DSAEK and nDSAEK increased corneal thickness on IOP readings obtained with one of the following four techniques: GAT, dynamic contour tonometry (DCT), non-contact pneumatonometry, and miniaturized digital electronic tonometry (Tono-Pen XL, or Tonopen).

Patients and Methods

This prospective, cross-sectional study was approved by the Ethical Committee of Kanazawa University Graduate School of Medical Science and complied with the tenets of the Declaration of Helsinki. We evaluated 24 eyes (22 patients: 6 men, 16 women; mean age, 74.0 years) that had undergone either successful DSAEK (11 eyes) or nDSAEK (13 eyes) treatment at least 3 months prior to testing (mean duration, 327.0 ± 167.4 days; range, 103–621 days). The causes of the corneal edema were post-argon laser iridotomy (17/24, 70.8%), followed by endothelitis (3/24, 12.5%), Fuchs dystrophy (2/24, 8.3%), pseudophakia (1/24, 4.2%), and pseudoexofoliation (1/24, 4.2%). Pseudoexofoliation syndrome is known to cause endothelial cell loss.[9] None of the patients had a previous glaucoma procedure. All surgeries were performed by a single surgeon (A. K.). DSAEK and nDSAEK procedures are described in detail by Kobayashi and Yokogawa and colleagues.[7,8,10] In brief, donor grafts for all 24 eyes were prepared with a microkeratome (ALTK Cbm, Moria, Antony, France) equipped with a 300-μm head and an 8.0-mm-diameter punch (Barron donor cornea punch, Katena Products, Denville, NJ, USA). In 14 of the 24 cases, simultaneous cataract procedures (phacoemulsification and intraocular lens implantation) were performed just prior to both the DSAEK and nDSAEK surgery. In the nDSAEK procedures, the Descemet's membrane scoring and stripping process was totally eliminated.

We excluded patients with clinically detectable corneal edema or other active corneal pathology such as an epithelial defect or infection. Each patient enrolled in the study underwent a comprehensive anterior segment evaluation. All corneas evaluated in this study were crystal clear, and none of the participants had corneal edema clinically detectable by slit-lamp biomicroscopy at the time of study evaluation.

All IOP measurements were performed by one of two authors (A. K., H. Y.). Pressure was measured with Goldmann applanation tonometry (GAT) and dynamic contour tonometry (DCT: PASCAL, Swiss Microtechnology, Zurich, Switzerland),[11,12] pneumatonometry (TX-F, Canon, Tokyo, Japan), and Tonopen (Tono-Pen XL; Mentor Massachusetts, Norwell, MA, USA). Measuring was conducted in the following sequence: pneumatonometry, GAT, DCT, and Tonopen. The time interval between measurements using each technique was about 5 min. Two measurements on average were obtained with each technique; additional measurements were performed only if the difference between the first and second measurements exceeded 2 mmHg. For DCT measurement, a DCT module was mounted onto a slit-lamp biomicroscope (30SL-M, Carl Zeiss Japan, Tokyo, Japan), after which a disposable sensor cap was attached. After the cornea was anesthetized, the measuring tip was aligned so that the pressure sensor was centered within the contact zone for 3–5 s. IOP readings and the quality of the measurement were displayed on the digital screen; a reading of quality (Q) 1 to Q3 (with Q1 the best) was considered acceptable. Poor readings (rated Q4 to Q5) were discarded, and the pressure was measured again. Central corneal thickness (CCT) was measured by ultrasonic pachymetry (DGH 500; DGH Technology, Exton, PA, USA). Three measurements on average were used for the analysis of total corneal thickness.

Bland-Altman plots were examined to assess agreement between each pair of measurement methods.[13] The mean pressure measurement for each pair of methods was plotted on the x axis, with the difference in measurements between methods plotted on the y axis. In brief, if the two measurements were nearly identical, the mean difference would be close to zero. In addition, correlations between CCT and pressure measurements were assessed.

Descriptive statistics were expressed as mean ± standard deviation (SD). For all analyses, P values of less than 0.05 were considered statistically significant. Sample size calculation was performed as described previously,[14] when IOP measured by DCT and GAT was compared.

Results

Pressure was consistently measured with good quality using DCT (all patients scored Q3 on the quality scale). In the DSAEK group, mean pressure measured by GAT was 14.4 ± 3.6 mmHg, by DCT 13.9 ± 3.0, by pneumatonometry 11.2 ± 3.6, and by Tonopen 13.2 ± 4.1. In the nDSAEK group, mean pressure measured by GAT was 15.0 ± 3.2 mmHg, by DCT 14.4 ± 2.5, by pneumatonometry 12.5 ± 3.2, and by Tonopen 14.4 ± 3.0.

Two-sided paired-difference t tests and Bland-Altman plots indicated that pressure measured by pneumatonometry was significantly and consistently lower than that obtained with the other three methods: GAT (DSAEK, $P < 0.001$; nDSAEK, $P < 0.001$), Tonopen (DSAEK, $P = 0.003$; nDSAEK, $P = 0.003$), and DCT (DSAEK, $P < 0.001$; nDSAEK, $P < 0.001$). This was true in both the DSAEK and nDSAEK groups (Figs. 1, 2).

In the DSAEK group, correlations between pressure and CCT (629 ± 86 μm; mean, 627 μm; range, 482–784 μm) were not statistically significant for any of the techniques: GAT ($r = 0.371$, $P = 0.262$), DCT ($r = 0.353$, $P = 0.287$), pneumatonometry ($r = 0.359$, $P = 0.278$), and Tonopen ($r = 0.107$, $P = 0.754$). The same insignificant findings were true for the nDSAEK group (CCT: 654 ± 40 μm; mean, 660 μm; range,

Jpn J Ophthalmol
Vol 55: 98–102, 2011

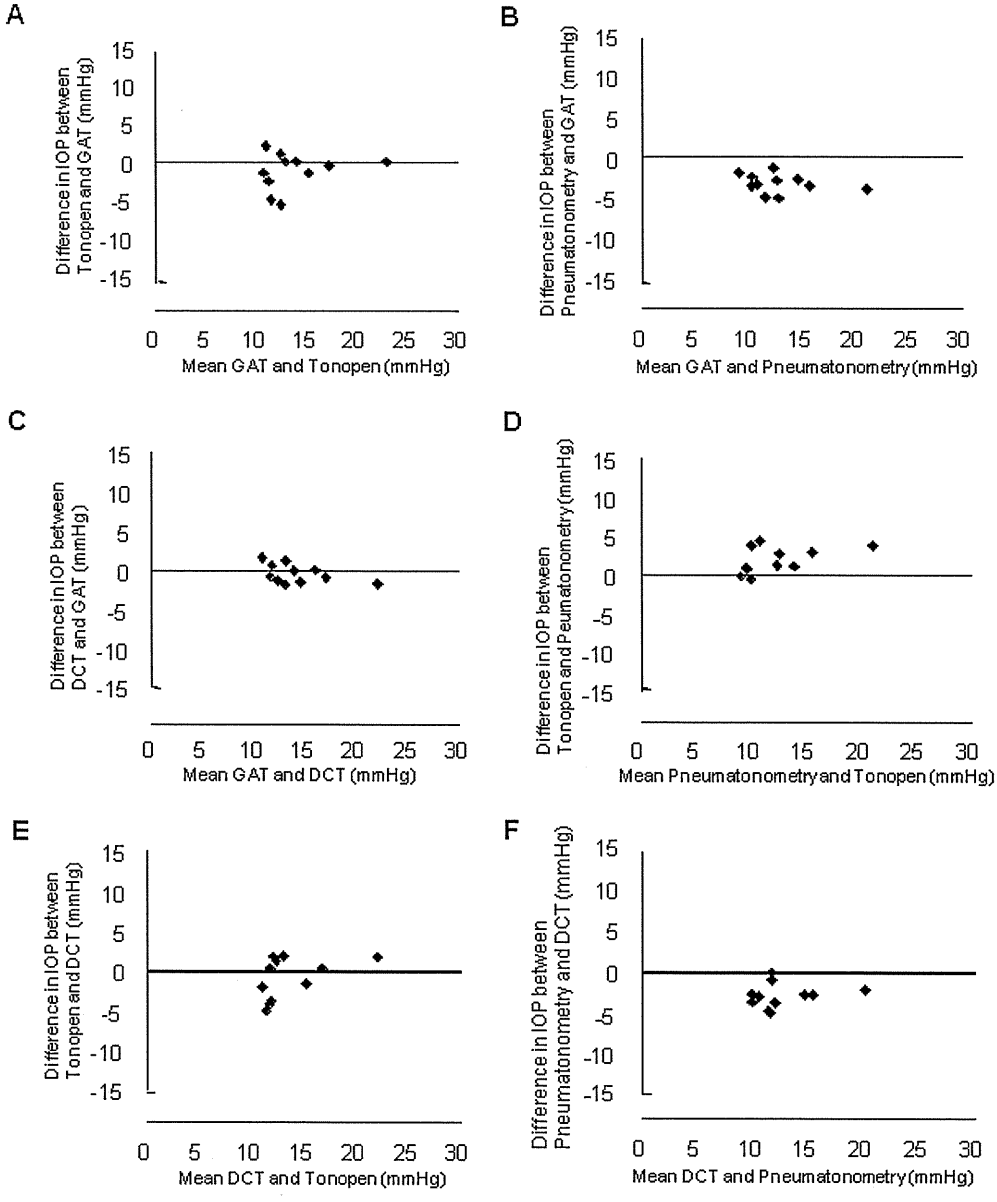

Figure 1A–F. Bland-Altman plots showing means of intraocular pressure (*IOP*) post-DSAEK as measured by two methods plotted against the difference in pressure measured by the same two methods. **A** GAT versus Tonopen (mean difference ± SD = –1.2 ± 2.4 mmHg; P = 0.113). **B** GAT versus pneumatonometry (mean difference ± SD = –3.2 ± 1.2 mmHg; $P < 0.001$). **C** GAT versus DCT (mean difference ± SD = –0.5 ± 1.2 mmHg, $P = 0.235$). **D** Pneumatonometry versus Tonopen (mean difference ± SD = 2.0 ± 1.7 mmHg; P = 0.003). **E** DCT versus Tonopen (mean difference ± SD = –0.8 ± 2.6 mmHg; $P = 0.337$). **F** DCT versus pneumatonometry (mean difference ± SD = –2.8 ± 1.4 mmHg; $P < 0.001$). Three pairs of measurement techniques (GAT versus pneumatonometry, pneumatonometry versus Tonopen, and DCT versus pneumatonometry) were significantly correlated. The remaining pairs (GAT versus Tonopen, GAT versus DCT, DCT versus Tonopen) were not statistically correlated. DSAEK, Descemet's stripping automated endothelial keratoplasty; *GAT*, Goldmann applanation tonometry; *DCT*, dynamic contour tonometry; *Tonopen*, Tono-Pen XL.

584–719 μm): GAT ($r = -0.169$, $P = 0.581$), DCT ($r = -0.272$, P = 0.369), pneumatonometry (r = 0.036, P = 0.906), and Tonopen ($r = -0.016$, $P = 0.959$).

Discussion

After DSAEK surgery, the cornea is significantly thicker than normal because of the microkeratome-dissected donor endothelial lamella, an approximately 100- to 200-μm-thick component of posterior stromal tissue, Descemet's membrane, and endothelium, all attached to the recipient's posterior corneal surface. Recently, successful elimination of the Descemet's membrane stripping process was documented for non-Fuchs-type bullous keratopathy (e.g., aniridia[15] and failed penetrating graft[16]). This procedure is termed nDSAEK,[7,8] and it has produced good clinical outcomes marked by superior visual acuity and minimal induced astigmatism for patients with argon laser iridotomy-induced bullous keratopathies.

Previously, researchers were unable to demonstrate correlations between CCT and IOP as measured by three techniques (GAT, pneumatonometry, and DCT) in DSAEK-treated eyes,[14] indicating that falsely elevated GAT readings, as expected for thick corneas, did not occur after DSAEK treatment. Similarly, in this study we did not find any correlation between CCT and IOP as measured by four different techniques in either the DSAEK or nDSAEK group, a result consistent with previous findings.[14] Taken together, these findings strongly suggest that high IOP readings by GAT, pneumatonometry, DCT, or Tonopen should raise a suspicion of an actually elevated pressure not only

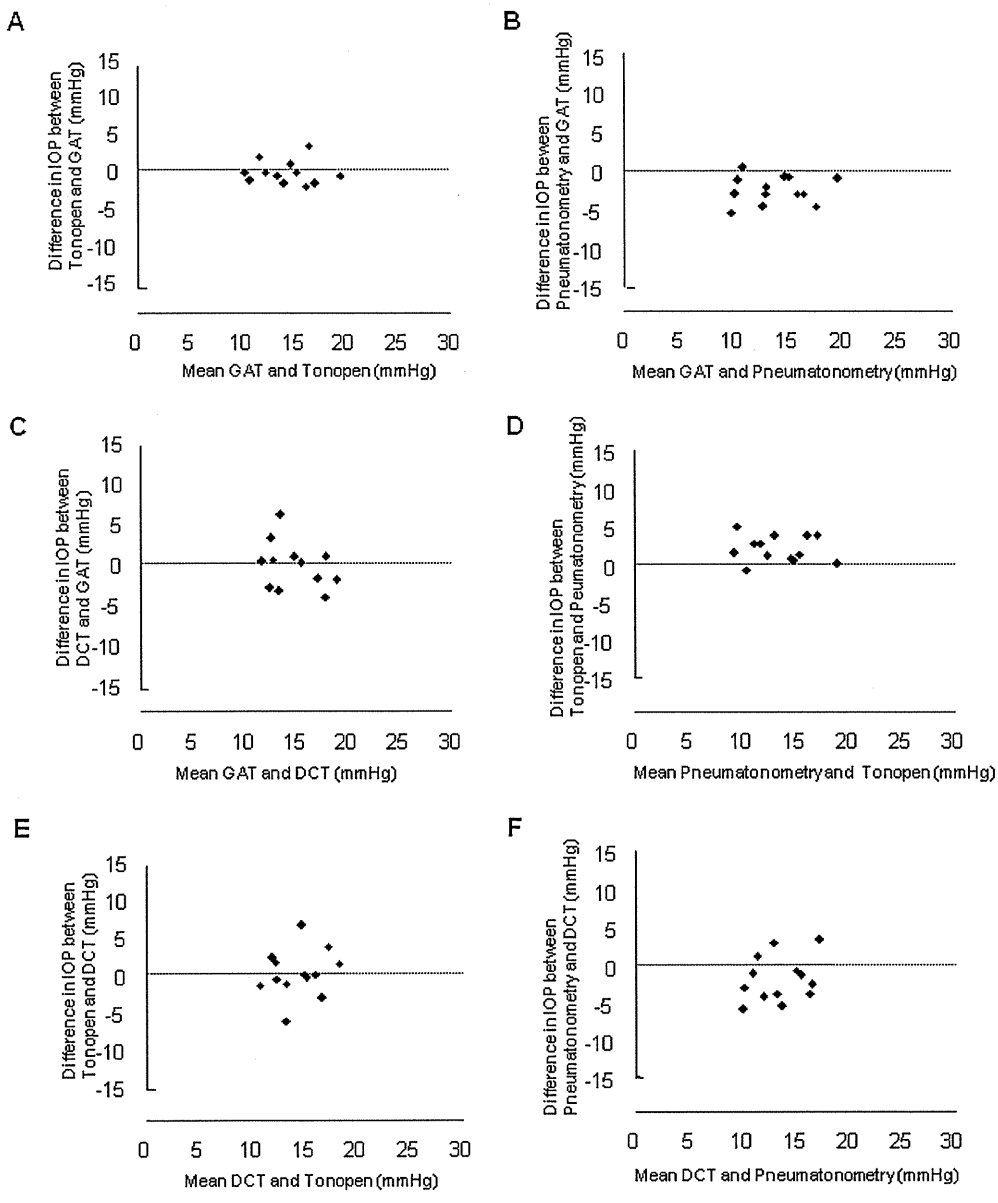

Figure 2A–F. Bland-Altman plots showing means of IOP post-nDSAEK as measured by two methods plotted against the difference in pressure measured by the same two methods. **A** GAT versus Tonopen (mean difference ± SD = –0.6 ± 1.5 mmHg; P = 0.188). **B** GAT versus pneumatonometry (mean difference ± SD = –2.5 ± 1.8 mmHg; $P < 0.001$). **C** GAT versus DCT (mean difference ± SD = –0.6 ± 2.9 mmHg; P = 0.504). **D** Pneumatonometry versus Tonopen (mean difference ± SD = 2.0 ± 1.7 mmHg; $P = 0.002$). **E** DCT versus Tonopen (mean difference ± SD = –0.0 ± 3.0 mmHg; $P = 0.980$). **F** DCT versus pneumatonometry (mean difference ± SD = –2.0 ± 3.0 mmHg; (P = 0.032). Three pairs of measurement techniques (GAT versus pneumatonometry, pneumatonometry versus Tonopen, and DCT versus pneumatonometry) were significantly correlated. The remaining pairs (GAT versus Tonopen, GAT versus DCT, DCT versus Tonopen) were not statistically correlated. nDSAEK, non-Descemet's stripping automated endothelial keratoplasty.

in DSAEK-treated eyes but also in nDSAEK-treated eyes. In other words, both DSAEK-treated and nDSAEK-treated thick corneas behave like normal corneas. Probably, the attached endothelial lamella on the posterior surface of the recipient cornea has little or no effect on the biomechanical properties of the preexisting cornea.

In this study, we showed that pressure measured by pneumatonometry was statistically lower than pressure measured with other techniques (GAT, DCT, and Tonopen); this finding was documented for both DSAEK- and nDSAEK-treated eyes (Figs. 1, 2). In contrast, there was no significant difference between GAT and DCT readings. Recently, Vajaranant and coworkers[14] investigated IOP after DSAEK treatment using three different techniques: GAT, pneumatonometry, and DCT. They reported that, unlike our results, pressure measurements by pneumatonometry and DCT were significantly higher than those obtained with GAT.[14] Previous studies have indicated that pressure readings obtained with DCT are higher than those obtained with GAT, with a range of 0.7–4.4 mmHg in eyes with normal corneas.[17–25] Also, one study reported that pneumatonometry measurements in study subjects treated with laser in situ keratomileusis (LASIK) were approximately 2 mmHg higher than those obtained with GAT.[26] We are unsure why our pressure readings obtained with pneumatonometry were lower than those obtained with the other techniques, or why DCT readings were not higher than the GAT readings. One possible reason is that the low number of patients in this study affected the statistical outcome. Another possible reason is that the presence of host Descemet's membrane or compressed host endothelium plays a role in the results obtained by pressure

measurements with pneumatonometry or DCT. Furthermore, the thinner mean CCT in our study (DSAEK, 629 ± 86 μm; nDSAEK, 654 ± 40 μm) compared with thicknesses reported by Vajaranant and coworkers (701 ± 68 μm)[14] might have influenced readings obtained with either pneumatonometry or DCT or both.

In conclusion, in both DSAEK- and nDSAEK-treated eyes, IOP readings by all four techniques (GAT, DCT, pneumatonometry, and Tonopen) might be independent of artificially enhanced corneal thickness in this small study. Further investigations using a larger number of patients are required to fully elucidate the relationship between intraocular pressure readings and treatment with DSAEK or nDSAEK.

References

1. Melles GR, Eggink FA, Lander F, et al. A surgical technique for posterior lamellar keratoplasty. Cornea 1998;17:618–626.
2. Terry MA, Ousley PJ. Small-incision deep lamellar endothelial keratoplasty (DLEK): six-month results in the first prospective clinical study. Cornea 2005;24:59–65.
3. Terry MA, Ousley PJ. Deep lamellar endothelial keratoplasty: visual acuity, astigmatism, and endothelial survival in a large prospective series. Ophthalmology 2005;112:1541–1548.
4. Price MO, Price FW Jr. Descemet's stripping with endothelial keratoplasty: comparative outcomes with microkeratome-dissected and manually dissected donor tissue. Ophthalmology 2006;113: 1936–1942.
5. Price FW Jr, Price MO. Descemet's stripping with endothelial keratoplasty in 200 eyes: early challenges and techniques to enhance donor adherence. J Cataract Refract Surg 2006;32:411–418.
6. Gorovoy MS. Descemet-stripping automated endothelial keratoplasty. Cornea 2006;25:886–889.
7. Kobayashi A, Yokogawa H, Sugiyama K. Non-Descemet stripping automated endothelial keratoplasty for endothelial dysfunction secondary to argon laser iridotomy. Am J Ophthalmol 2008;146: 543–549.
8. Kobayashi A, Yokogawa H, Sugiyama K. In vivo laser confocal microscopy findings after non-Descemet stripping automated endothelial keratoplasty. Ophthalmology 2009;116:1306–1313.
9. Miyake K, Matsuda M, Inaba M. Corneal endothelial changes in pseudoexfoliation syndrome. Am J Ophthalmol 1989;108:49–52.
10. Kobayashi A, Mawatari Y, Yokogawa H, Sugiyama K. In vivo laser confocal microscopy after Descemet's stripping with automated endothelial keratoplasty. Am J Ophthalmol 2008;145:977–985.
11. Punjabi OS, Kniestedt C, Stamper RL, Lin SC. Dynamic contour tonometry: principle and use. Clin Experiment Ophthalmol 2006;34:837–840.
12. Herndon LW. Measuring intraocular pressure-adjustments for corneal thickness and new technologies. Curr Opin Ophthalmol 2006;17:115–119.
13. Bland JM, Altman DG. Statistical methods for assessing agreement between two methods of clinical measurement. Lancet 1986;1: 307–310.
14. Vajaranant TS, Price MO, Price FW, et al. Intraocular pressure measurements following Descemet stripping endothelial keratoplasty. Am J Ophthalmol 2008;145:780–786.
15. Price MO, Price FW Jr, Trespalacios R. Endothelial keratoplasty technique for aniridic aphakic eyes. J Cataract Refract Surg 2007;33:376–379.
16. Price FW Jr, Price MO. Endothelial keratoplasty to restore clarity to a failed penetrating graft. Cornea 2006;25:895–899.
17. Schneider E, Grehn F. Intraocular pressure measurement—comparison of dynamic contour tonometry and Goldmann applanation tonometry. J Glaucoma 2006;15:2–6.
18. Herdener S, Pache M, Lautebach S, Funk J. Dynamic contour tonometry versus Goldmann applanation tonometry—a comparison of agreement and reproducibility. Graefes Arch Clin Exp Ophthalmol 2007;245:1027–1030.
19. Doyle A, Lachkar Y. Comparison of dynamic contour tonometry with Goldmann applanation tonometry over a wider range of central corneal thickness. J Glaucoma 2005;14:288–292.
20. Francis BA, Hsieh A, Lai M, et al. Effects of corneal thickness, corneal curvature, and intraocular pressure level on Goldmann applanation tonometry and dynamic contour tonometry. Ophthalmology 2007;114:20–26.
21. Martinez JM, Garcia-Feijoo J, Vico E, et al. Effect of corneal thickness on dynamic contour, rebound, and Goldmann tonometry. Ophthalmology 2006;113:2156–2162.
22. Barleon L, Hoffman EM, Berres M, et al. Comparison of dynamic contour tonometry and Goldmann applanation in glaucoma patients and healthy subjects. Am J Ophthalmol 2006;142: 583–590.
23. Kniestedt C, Lin S, Choe J, et al. Clinical comparison of contour and applanation tonometry and their relationship to pachymetry. Arch Ophthalmol 2005;123:1532–1537.
24. Medeiros FA, Sample PA, Weinreb RN. Comparison of dynamic contour tonometry and Goldmann applanation tonometry in African-American subjects. Ophthalmology 2007;114:658–665.
25. Salvetat ML, Zeppieri M, Tosoni C, Brusini P. Comparisons between PASCAL dynamic tonometry, the tonopen, and Goldmann applanation tonometry in patients with glaucoma. Acta Ophthalmol Scand 2007;85:272–279.
26. Zadok D, Tran D, Twa M, et al. Pneumotonometric versus Goldmann tonometry after laser in situ keratomileusis for myopia. J Cataract Refract Surg 1999;25:1344–1348.

Hormonal Regulation of Na^+/K^+-Dependent ATPase Activity and Pump Function in Corneal Endothelial Cells

Shin Hatou, MD†*

Abstract: Na^+- and K^+-dependent ATPase (Na,K-ATPase) in the basolateral membrane of corneal endothelial cells plays an important role in the pump function of the corneal endothelium. We investigated the role of dexamethasone in the regulation of Na,K-ATPase activity and pump function in these cells. Mouse corneal endothelial cells were exposed to dexamethasone or insulin. ATPase activity was evaluated by spectrophotometric measurement, and pump function was measured using an Ussing chamber. Western blotting and immunocytochemistry were performed to measure the expression of the Na,K-ATPase α1-subunit. Dexamethasone increased Na,K-ATPase activity and the pump function of endothelial cells. Western blot analysis indicated that dexamethasone increased the expression of the Na,K-ATPase α_1-subunit but decreased the ratio of active to inactive Na,K-ATPase α_1-subunit. Insulin increased Na,K-ATPase activity and pump function of cultured corneal endothelial cells. These effects were transient and blocked by protein kinase C inhibitors and inhibitors of protein phosphatases 1 (PP1) and 2A (PP2A). Western blot analysis indicated that insulin decreased the amount of inactive Na,K-ATPase α_1-subunit, but the expression of total Na,K-ATPase α_1-subunit was unchanged. Immunocytochemistry showed that insulin increased cell surface expression of the Na,K-ATPase α_1-subunit. Our results suggest that dexamethasone and insulin stimulate Na,K-ATPase activity in mouse corneal endothelial cells. The effect of dexamethasone activation in these cells was mediated by Na,K-ATPase synthesis and an increased enzymatic activity because of dephosphorylation of Na,K-ATPase α_1-subunits. The effect of insulin is mediated by the protein kinase C, PP1, and/or PP2A pathways.

Key Words: corneal endothelium, insulin, ouabain, protein kinase C, protein phosphatase, Na^+- and K^+-dependent ATPase

(*Cornea* 2011;30(Suppl. 1):S60–S66)

A single layer of endothelial cells in a well-arranged mosaic pattern covers the posterior surface of the Descemet membrane in the cornea.[1] Corneal hydration is primarily determined by the balance between penetration of the aqueous humor across the corneal endothelium into the stroma and subsequent pumping of the fluid out of the stroma. The accumulation of fluid in the stroma resulting from disturbance of this balance may lead to bullous keratopathy, which is characterized by an edematous cornea with reduced transparency.[2]

Total pumping activity for the removal of fluid from the cornea is determined by the number of endothelial cells and the pump function of each cell. Given that human corneal endothelial cells have a limited proliferative capacity, endothelial dystrophies, ocular trauma, corneal graft rejection, and insults associated with intraocular surgeries may result in corneal endothelial cell loss and permanent damage. Replacement of the corneal endothelium by keratoplasty is currently the only established therapeutic approach for recovery of endothelial cell number. Pseudophakic or aphakic bullous keratopathy, Fuchs endothelial dystrophy, and failed corneal grafts remain common indications for keratoplasty, accounting for approximately 60% of the total number of such procedures.[3–5] Activation of the pump function in the remaining endothelial cells is a potential alternative approach to recovery of the total pumping activity in the cornea, so long as the total number of such cells is within an acceptable range. However, therapeutic approaches to the activation of corneal endothelial cells remain to be established.

The Na^+- and K^+-dependent ATPase (Na,K-ATPase) expressed in the basolateral membrane of corneal endothelial cells is primarily responsible for the pump function of the corneal endothelium.[1] The Na,K-ATPase pump site density in the corneal endothelium was found to be increased in eyes affected by moderate guttata.[6] Na,K-ATPase pump site density showed an initial increase, a sudden marked decrease, and a subsequent gradual decline associated with the end stage of disease in patients with Fuchs endothelial dystrophy.[7] These observations indicate that certain conditions can induce a compensatory increase in Na,K-ATPase pump site density and, presumably, in endothelial pump function. They also suggest the existence of a regulatory mechanism, or mechanisms, for the control of total Na,K-ATPase activity in the corneal endothelium.

Several studies have shown that glucocorticoids stimulate Na,K-ATPase activity through multiple complex mechanisms, including gene expression, transcription, translocation, and enzymatic activity, in a variety of tissues.[8] Although the results of experimental studies concerning the effects of glucocorticoids on corneal endothelial damage do not show any close correlations,[9–11] topical glucocorticoids have been clinically used for the treatment of corneal

From the *Division for Vision Research, National Institute of Sensory Organs, National Tokyo Medical Center, Tokyo, Japan; and †Department of Ophthalmology, Keio University School of Medicine, Tokyo, Japan.

Supported in part by a grant from the Ministry of Health, Labour and Welfare (Japan).

The author has no financial or conflicts of interest to disclose.

Reprints: Shin Hatou, Department of Ophthalmology, Keio University School of Medicine, 35 Shinanomachi, Shinjuku-ku, Tokyo 160-8582, Japan (e-mail: tr97469@zc4.so-net.ne.jp).